Parity Symmetry-Breaking Phase Transition in a Nonlinear Rabi-Hubbard Lattice

M.Sc. Thesis

Ari Pyykkönen
University of Oulu
Research Center for Molecular Materials
Division of Theoretical Physics

2015

Abstract

Lattices consisting of cavity QED and circuit QED elements have come under focus as a platform for studying several novel quantum phenomena. In particular, a lattice of Rabi systems described by the Rabi-Hubbard model is expected to display a new Z_2 parity symmetry-breaking phase transition of light between a Rabi insulator and a delocalized superradiant phase. In this thesis, we examine a superconducting circuit called the artificial trapped ion as a means to realize a nonlinear Rabi-Hubbard lattice. We use mean field theory and second-order perturbation theory to derive an expression for the boundary of the phase transition and calculate it numerically. We show that nonlinearity in the light-matter coupling results in nontrivial behavior for the phase boundary, in the form of a peak arising at a certain strength of the nonlinearity. We also see a behavior of oscillation followed by saturation as the nonlinearity increases.

Contents

Chapter 1

Introduction

Lattices made of cavity or circuit QED systems are expected to exhibit novel quantum phenomena, such as phase transitions of light between Mott-like insulating and superfluid phases. Proposals to realize artificial gauge fields and quantum Hall fluids of light have also been made [1, 2]. In a system called the Rabi-Hubbard model, the individual lattice sites are described using the full Rabi Hamiltonian rather than an approximation such as in the Jaynes-Cummings-Hubbard model [3]. This kind of system has not been studied extensively, but it has been discussed in the context of linear single-site couplings [4–7].

In this study, we investigate the effects of nonlinearities in the single-site coupling on the Rabi-Hubbard model, which can be experimentally realized as a lattice of (artificial) trapped ions. We propose to use the so-called LSET topology [8], in which the coupling is created via nonlinear Josephson elements. So far, only classical simulations have been conducted for lattices consisting of nonlinearly coupled Rabi and Jaynes-Cummings systems [9]. Primarily, we are interested in the effects of nonlinearity on the Z_2 parity symmetry-breaking order-disorder phase transition of the lattice within the mean field approximation. We will study this by calculating the phase boundary numerically, utilizing perturbation theory.

We begin with the basic concepts of the quantum harmonic oscillator and how it relates to the quantum mechanical description of electromagnetic radiation. Next we review cavity and circuit QED to provide background for past studies involving the Rabi-Hubbard model. We continue on to real and artificial trapped ions as a mathematical extension of CQED into the nonlinear regime. Finally, we review the Rabi-Hubbard model in light of mean field theory and calculate the formula for the phase boundary using

second-order perturbation theory. The result can be directly generalized to the nonlinear case, as we will see.

Chapter 2

Quantum Nature of Light

The interaction of light and matter is of great interest in quantum optics, and plays an important part in the Rabi-Hubbard model. Quantum effects are vital in the systems involved, and the classical theory of electromagnetism will not be sufficient. We will therefore begin by quantizing the electromagnetic field. It will turn out that each mode of the field corresponds to a quantum harmonic oscillator, and the whole field can be treated a collection of independent harmonic oscillators.

2.1 Quantum Harmonic Oscillator

Let us begin with the equations for a simple classical harmonic oscillator and follow the discussion by Thuneberg [10] in the quantization. They are

$$\dot{p} = -m\omega_0^2 q \tag{2.1a}$$

$$\dot{q} = \frac{p}{m}, \tag{2.1b}$$

where q is the spatial coordinate, p is the momentum, $\omega_0 = \sqrt{k/m}$, k is the spring constant and m is the mass of the oscillator. The energy can be written as the sum of the kinetic and potential energies

$$E = \frac{p^2}{2m} + \frac{1}{2}m\omega_0^2 q^2. \tag{2.2}$$

To move to the quantum mechanical picture, q and p must be replaced with the corresponding Hermitian operators that satisfy the commutation relation

$$[q, p] = i\hbar. \tag{2.3}$$

Now, let us define the operators a and $a^\dagger$,

$$a = \frac{1}{\sqrt{2\hbar}}(\sqrt{m\omega_0}q + i\frac{p}{\sqrt{m\omega_0}}) \tag{2.4a}$$

$$a^\dagger = \frac{1}{\sqrt{2\hbar}}(\sqrt{m\omega_0}q - i\frac{p}{\sqrt{m\omega_0}}). \tag{2.4b}$$

A direct calculation shows that

$$[a, a] = [a^\dagger, a^\dagger] = 0, \quad [a, a^\dagger] = 1. \tag{2.5}$$

To gain an interpretation for a and $a^\dagger$, we will study the operator

$$\hat{n} = a^\dagger a. \tag{2.6}$$

Because $\hat{n}^\dagger = (a^\dagger a)^\dagger = a^\dagger (a^\dagger)^\dagger = a^\dagger a = \hat{n}$, $\hat{n}$ is Hermitian, which means its eigenvalues are real valued and its eigenvectors are orthogonal. We will label the eigenstates of $\hat{n}$ by using the (real) eigenvalues n

$$\hat{n}\,|n\rangle = n\,|n\rangle\,. \tag{2.7}$$

We will assume the states $|n\rangle$ are normalized. The eigenvalue n cannot be negative:

$$\begin{aligned} n = \langle n|\hat{n}|n\rangle = \langle n|a^\dagger a|n\rangle = \sum_m \langle n|a^\dagger|m\rangle \langle m|a|n\rangle = \sum_m |\langle m|a|n\rangle|^2 \\ \geq 0. \end{aligned} \tag{2.8}$$

From (2.5), we can calculate

$$[\hat{n}, a] = -a. \tag{2.9}$$

This leads to the relation

$$\hat{n}(a\,|n\rangle) = a\hat{n}\,|n\rangle - a\,|n\rangle = na\,|n\rangle - a\,|n\rangle = (n-1)(a\,|n\rangle). \tag{2.10}$$

We can therefore see that $a\,|n\rangle$ is either an eigenvector of $\hat{n}$ corresponding to the eigenvalue $n-1$ or $a\,|n\rangle = 0$. The latter implies that $\hat{n}\,|n\rangle = 0$ and $n = 0$. In the former case we have

$$a\,|n\rangle = c\,|n-1\rangle\,, \tag{2.11}$$

where c is determined by normalization:

$$n = \langle n|a^\dagger a|n\rangle = c^* c\,\langle n-1|n-1\rangle = |c|^2. \tag{2.12}$$

We can now fix

$$a\,|n\rangle = \sqrt{n}\,|n-1\rangle\,. \tag{2.13}$$

If one operates on the state $|n\rangle$ sufficiently many times with the operator a, one should eventually arrive at negative eigenvalues, which contradicts (2.8). The only way this does not happen is if n is an integer, since then $a\,|0\rangle = 0$ and the process ends. Similarly, one can deduce for $a^\dagger$

$$a^\dagger\,|n\rangle = \sqrt{n+1}\,|n+1\rangle\,. \tag{2.14}$$

We thus have an interpretation for a and $a^\dagger$: a removes one quantum and $a^\dagger$ adds one. Because of these properties, a and $a^\dagger$ are called the annihilation operator and the creation operator, respectively. The states

$$|n\rangle\,, \quad n = 0, 1, 2, \ldots, \infty \tag{2.15}$$

are known as number states or Fock states.

The energy of the classical oscillator was (2.2)

$$E = \frac{p^2}{2m} + \frac{1}{2}m\omega_0^2 q^2.$$

The Hamiltonian of the quantum harmonic oscillator is of the same form, with q and p replaced with the corresponding operators as mentioned before,

$$H = \frac{p^2}{2m} + \frac{1}{2}m\omega_0^2 q^2. \tag{2.16}$$

We can write this in terms of the annihilation and creation operators a and $a^\dagger$ by inverting equations (2.4) and inserting them in (2.16). The result is

$$H = \hbar\omega_0\Big(a^\dagger a + \frac{1}{2}\Big). \tag{2.17}$$

The eigenvalues and eigenstates can now easily be found. Operating on the number states (2.15) with the Hamiltonian (2.17) gives

$$H\,|n\rangle = \hbar\omega_0\Big(a^\dagger a + \frac{1}{2}\Big)\,|n\rangle = \hbar\omega_0\Big(n + \frac{1}{2}\Big)\,|n\rangle = E_n\,|n\rangle\,. \tag{2.18}$$

This directly tells us that the eigenstates of the Hamiltonian are the states $|n\rangle$ and the eigenvalues are

$$E_n = \hbar\omega_0\Big(n + \frac{1}{2}\Big). \tag{2.19}$$

The quantum harmonic oscillator has discrete energy levels as multiples of $\hbar\omega_0$. The quantum number n can be interpreted as the number of quanta in

the oscillator, and the zero-point energy $E_0 = \hbar\omega_0/2$ corresponds to $n = 0$ (the state $|0\rangle$), where no quanta are present. The operator $\hat{n} = a^\dagger a$ is called the number operator, since it gives the number of quanta in the oscillator. It should be noted that all eigenstates can be generated from the zero-state with the creation operator $a^\dagger$ as

$$|n\rangle = \frac{(a^\dagger)^n}{\sqrt{n!}} |0\rangle . \tag{2.20}$$

2.2 Quantization of the Electromagnetic Field

As in Ref. [11], we will begin by considering the classical field equations describing the free electromagnetic field. The Maxwell equations in the absence of sources are

$$\boldsymbol{\nabla} \cdot \mathbf{B} = 0 \tag{2.21a}$$

$$\boldsymbol{\nabla} \times \mathbf{E} = -\frac{\partial \mathbf{B}}{\partial t} \tag{2.21b}$$

$$\boldsymbol{\nabla} \cdot \mathbf{D} = 0 \tag{2.21c}$$

$$\boldsymbol{\nabla} \times \mathbf{H} = \frac{\partial \mathbf{D}}{\partial t}, \tag{2.21d}$$

with the constitutive equations

$$\mathbf{B} = \mu_0 \mathbf{H} \tag{2.22a}$$

$$\mathbf{D} = \epsilon_0 \mathbf{E}, \tag{2.22b}$$

where $\mathbf{D}$ and $\mathbf{B}$ are the electric and magnetic flux densities, $\mathbf{E}$ and $\mathbf{H}$ are the electric and magnetic fields, and μ_0 and ϵ_0 are the magnetic and electric permittivity of free space. For the speed of light in vacuum we also have $c = 1/\sqrt{\mu_0 \epsilon_0}$. These fields are gauge invariant, which means that the scalar potential can always be made to vanish and $\mathbf{B}$ and $\mathbf{E}$ can be determined from the vector potential $\mathbf{A}$ as

$$\mathbf{B} = \boldsymbol{\nabla} \times \mathbf{A} \tag{2.23a}$$

$$\mathbf{E} = -\frac{\partial \mathbf{A}}{\partial t}. \tag{2.23b}$$

Using the Coulomb gauge giving the condition

$$\boldsymbol{\nabla} \cdot \mathbf{A} = 0, \tag{2.24}$$

and substituting equations (2.23) into the last of the equations (2.21) results in the wave equation for $\mathbf{A}(\mathbf{r},t)$,

$$\nabla^2\mathbf{A}(\mathbf{r},t) = \frac{1}{c^2}\frac{\partial^2\mathbf{A}(\mathbf{r},t)}{\partial t^2}. \tag{2.25}$$

Note that the wave equations for $\mathbf{B}$ and $\mathbf{E}$ can be recovered by taking the curl and time derivative, respectively, of equation (2.25).

Let us now separate the vector potential into two complex terms

$$\mathbf{A}(\mathbf{r},t) = \mathbf{A}^{(+)}(\mathbf{r},t) + \mathbf{A}^{(-)}(\mathbf{r},t), \tag{2.26}$$

where $\mathbf{A}^{(+)}(\mathbf{r},t)$ contains the amplitudes that vary as $e^{-i\omega t}$ with frequency $\omega > 0$ and $\mathbf{A}^{(-)}(\mathbf{r},t)$ contains the amplitudes that vary as $e^{i\omega t}$. In addition, $\mathbf{A}^{(-)} = (\mathbf{A}^{(+)})^*$. We will describe the field restricted to a certain volume of space and expand the vector potential in terms of discrete orthonormal mode functions $\mathbf{u}_k(\mathbf{r})$:

$$\mathbf{A}^{(+)}(\mathbf{r},t) = \sum_k c_k\mathbf{u}_k(\mathbf{r})e^{-i\omega_k t}, \tag{2.27}$$

where the coefficients c_k are constant. The mode functions $\mathbf{u}_k(\mathbf{r})$ will satisfy the wave equation

$$\left(\nabla^2 + \frac{\omega_k^2}{c^2}\right)\mathbf{u}_k(\mathbf{r}) = 0. \tag{2.28}$$

In addition, they satisfy the transversality condition

$$\boldsymbol{\nabla}\cdot\mathbf{u}_k(\mathbf{r}) = 0 \tag{2.29}$$

and the orthonormality condition

$$\int \mathbf{u}_k^*(\mathbf{r})\mathbf{u}_{k'}(\mathbf{r})d\mathbf{r} = \delta_{kk'}. \tag{2.30}$$

The mode functions depend on the boundary conditions of the physical volume being considered. For instance, periodic boundary conditions are appropriate for traveling waves while the conditions of reflecting walls lead to standing waves. With equation (2.27) and the corresponding equation for $\mathbf{A}^{(-)}(\mathbf{r},t)$, the vector potential can be written in the form

$$\mathbf{A}(\mathbf{r},t) = \sum_k \sqrt{\frac{\hbar}{2\omega_k\epsilon_0}}\left[a_k\mathbf{u}_k(\mathbf{r})e^{-i\omega_k t} + a_k^\dagger\mathbf{u}_k^*(\mathbf{r})e^{i\omega_k t}\right] \tag{2.31}$$

and the electric field in the form

$$\mathbf{E}(\mathbf{r},t) = i\sum_k \sqrt{\frac{\hbar\omega_k}{2\epsilon_0}}\left[a_k\mathbf{u}_k(\mathbf{r})e^{-i\omega_k t} - a_k^\dagger\mathbf{u}_k^*(\mathbf{r})e^{i\omega_k t}\right]. \tag{2.32}$$

The factors have been chosen so that a and $a^\dagger$ are dimensionless.

In classical electrodynamics, a and $a^\dagger$ are complex numbers. We accomplish the quantization of the electromagnetic field by choosing them to be mutually adjoint operators. Since photons are bosons, we choose the boson commutation relations

$$[a_k, a_{k'}] = [a_k^\dagger, a_{k'}^\dagger] = 0, \quad [a_k, a_{k'}^\dagger] = \delta_{kk'}. \tag{2.33}$$

The classical energy of the electromagnetic field is

$$\mathcal{E} = \frac{1}{2}\int (\epsilon_0 E^2 + \mu_0 H^2) d\mathbf{r}, \tag{2.34}$$

so we can construct the Hamiltonian by substituting (2.32) and the equivalent expression for $\mathbf{H}$ into (2.34). By making use of the conditions (2.29) and (2.30), the Hamiltonian is reduced to the form

$$H = \sum_k \hbar\omega_k \Big(a_k^\dagger a_k + \frac{1}{2}\Big). \tag{2.35}$$

This is of the same form as the Hamiltonian for a collection of independent harmonic oscillators with frequencies ω_k. We can therefore treat each mode of the electromagnetic field as a harmonic oscillator with the number operator $\hat{n}_k = a_k^\dagger a_k$ telling us the number of photons occupying that mode. Based on (2.33) and (2.35), we identify a_k and $a_k^\dagger$ as the annihilation and creation operators of the mode, with a_k destroying a photon and $a_k^\dagger$ creating one. [11]

Chapter 3

CQED and Ion Traps

The interaction of a two-level atom with a single-mode quantized field is one of the most basic models in quantum optics. It is known as the Rabi model or, under the rotating wave approximation, the Jaynes-Cummings model. Its realizations include cavity and circuit quantum electrodynamics (CQED) and, for nonlinear couplings, ion traps.

Cavity quantum electrodynamics, in which atoms are coupled to discrete photon modes inside a cavity, are of great interest in the study of fundamental quantum mechanics in open systems, especially relating to quantum coherence, measurement, entanglement and nonlocality. Cavity QED systems with strong coupling have also been proposed as possible candidates for quantum information processing and transmission, and experiments with such systems provide support for the development of technologies such as quantum computation and communication. [12, 13]

Cavity QED analogs utilizing superconducting electric circuits, of which we will present a system involving a Cooper pair box inside a co-planar microwave resonator, provide new avenues for the development of quantum computation and the study of quantum phenomena with macroscopic objects. [12, 14]

Ion trap technology with single trapped ions and other charged particles has contributed significantly to many fields in physics, such as the effort to gain complete control over quantum coherence in isolated systems. It is also possible to trap and cool an ion close to its vibrational ground state, prepare complex superpositions of energy eigenstates with optical excitation and observe the resulting dynamics with good sensitivity. Current practical applications include the ability to define time standards using ion trap clocks. Ion trap technology shows particular promise in the field of quantum

information processing since it has proven to be one of the most successful ways of creating and manipulating entangled states. Even if a quantum computer is not built using ion traps, they are accessible for testing concepts that might be applicable to other systems. [11, 15]

As for cavity QED, it is possible to construct circuit analogs for ion traps. We will examine a single Cooper pair transistor, SCPT, (also called superconducting single-electron transistor, SSET) coupled nonlinearly with an LC resonator and show that its Hamiltonian is equivalent to an ion trap with a quadrupolar trapping potential. Such a system may be realized using the LSET (inductive single-electron transistor) topology [8], and has been a subject of study in recent years [16–18]. The advantage of using circuit analogs instead of real cavity QED and ion traps lies in the accessibility of the systems and fact that they allow greater control over experimental parameters.

3.1 CQED

We will now briefly study cavity quantum electrodynamics and circuit quantum electrodynamics, in which a single mode of the electromagnetic field in a cavity interacts with a two-level dipole emitter.

3.1.1 Cavity Quantum Electrodynamics

In cavity QED, the system to be studied consists of a single two-level atom inside an optical cavity. The setup is sketched in figure 3.1. The main difficulty in realizing such a system experimentally arises from finding a way to localize a single two-level atom in the cavity for long periods of time. Several methods have been developed to accomplish this. One approach is to trap and cool two-level atoms in a magneto-optical trap and let them fall into a high-finesse cavity directly below it. At most one atom will then slowly fall through the cavity at a time. Another method is to use constraining forces to trap a single atom in the cavity. This can be done, for example, by using an ion trap scheme. [11]

The Hamiltonian describing the radiation field coupled to the atom is within the often used rotating wave approximation the Jaynes-Cummings Hamiltonian [12, 19, 20]

$$H = H_c + H_a + H_{\text{int}} = \hbar\omega_c a^\dagger a + \frac{\hbar\omega_a}{2}\sigma_z + \hbar g(\sigma_+ a + \sigma_- a^\dagger), \tag{3.1}$$

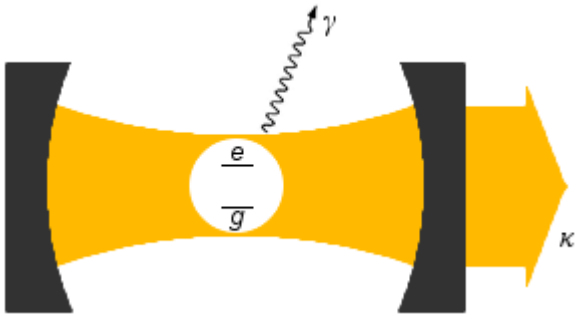

Figure 3.1: Two-level atom with ground state g and excited state e in an optical cavity. The atom is coupled to a single cavity mode of the electromagnetic field, but can emit photons into external modes at rate γ. The rate κ describes photon loss through the end mirror of the cavity.

where ω_c is the resonant frequency of the cavity and ω_a is the frequency spacing between the two states of the atom. It was originally introduced by Jaynes and Cummings [21]. The eigenproblem of the Jaynes-Cummings Hamiltonian has an analytical solution. The strength of the coupling between the radiation field and the atom at position $\mathbf{r}$ is determined by

$$g = \sqrt{\frac{\mu^2 \omega_c}{2\hbar\epsilon_0 V_m}} U(\mathbf{r}) = g_0 U(\mathbf{r}), \tag{3.2}$$

where μ is the dipole moment of the atom, $U(\mathbf{r})$ is the cavity standing wave mode function and the cavity mode volume V_m is defined by

$$V_m = \int |U(\mathbf{r})|^2 d\mathbf{r}. \tag{3.3}$$

The Jaynes-Cummings form of the cavity QED Hamiltonian originates from the model introduced by Rabi [4, 22], in which the Hamiltonian of a radiation field coupled to a two-level system is

$$H = \hbar\omega_c a^\dagger a + \frac{\hbar\omega_a}{2}\sigma_z + \hbar g(a^\dagger + a)(\sigma_+ + \sigma_-). \tag{3.4}$$

The last term contains rotating terms $\sigma_+ a$ and $\sigma_- a^\dagger$, and counter-rotating terms $\sigma_+ a^\dagger$ and $\sigma_- a$. The latter do not conserve the total number of excitations

$$\mathcal{N} = a^\dagger a + \sigma_+ \sigma_-, \tag{3.5}$$

and are discarded within the rotating wave approximation. This leads to the Jaynes-Cummings Hamiltonian discussed above.

In the Jaynes-Cummings Hamiltonian of cavity QED (3.1) and the Rabi model (3.4), the first term on the right-hand side represents the electromagnetic mode, where we have neglected the zero-point energy. The second term is the Hamiltonian for the two-level system (qubit), and the last is the coupling term. We have used the Pauli spin matrices

$$\sigma_x = \begin{pmatrix} 0 & 1 \\ 1 & 0 \end{pmatrix}, \quad \sigma_y = \begin{pmatrix} 0 & -i \\ i & 0 \end{pmatrix}, \quad \sigma_z = \begin{pmatrix} 1 & 0 \\ 0 & -1 \end{pmatrix} \tag{3.6}$$

and the raising and lowering operators of the qubit,

$$\sigma_+ = \begin{pmatrix} 0 & 1 \\ 0 & 0 \end{pmatrix}, \quad \sigma_- = \begin{pmatrix} 0 & 0 \\ 1 & 0 \end{pmatrix}, \tag{3.7}$$

whose effect on the ground and excited states $|g\rangle$ and $|e\rangle$ of the qubit is

$$\sigma_+ |g\rangle = |e\rangle, \quad \sigma_+ |e\rangle = 0, \tag{3.8a}$$

$$\sigma_- |g\rangle = 0, \quad \sigma_- |e\rangle = |g\rangle. \tag{3.8b}$$

The Jaynes-Cummings Hamiltonian (3.1) operates in the direct product of the qubit space and the harmonic oscillator space. It has a basis formed by $|\alpha, n\rangle$, where $\alpha = g, e$ and $n = 0, 1, 2, \ldots, \infty$. [10, 11, 19, 20]

Note that in equation (3.1), the zero of the energy of the qubit is defined to be exactly between the two levels, giving H_a in matrix form as

$$H_a = \frac{\hbar\omega_a}{2}\sigma_z = \begin{pmatrix} \frac{\hbar\omega_a}{2} & 0 \\ 0 & -\frac{\hbar\omega_a}{2} \end{pmatrix}. \tag{3.9}$$

If the zero is instead set at the ground state, we can rewrite H_a with the lowering and raising operators as

$$H_a = \hbar\omega_a\sigma_+\sigma_- = \begin{pmatrix} \hbar\omega_a & 0 \\ 0 & 0 \end{pmatrix}, \tag{3.10}$$

thus removing the need for the Pauli spin matrices. The choice of zero energy is arbitrary and should have no effect on the physics of the system.

3.1.2 Circuit Quantum Electrodynamics

In circuit QED, we study a system comprised of a superconducting Cooper pair box inside a co-planar microwave resonator. A Cooper pair box consists

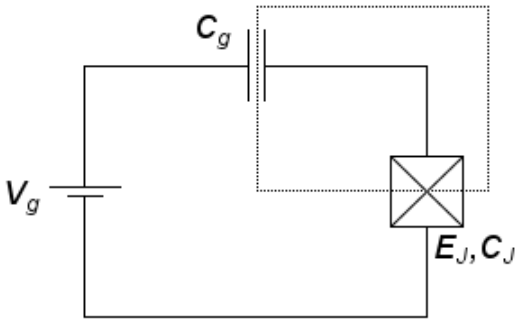

Figure 3.2: Circuit diagram of a Cooper pair box. The island (dotted line) is formed by the electrode between the gate capacitance and the Josephson junction. In the figure, V_g is the voltage applied to the island, E_J is the Josephson element coupling energy and C_g is the gate capacitance. The Josephson junction also contains an additional capacitance C_J.

of a metallic superconducting island coupled to a superconducting reservoir by a Josephson junction. A Josephson junction is composed of two superconductors coupled by a weak link, such as an insulator, which the Cooper pairs formed by electrons in a superconducting state can tunnel through. See section 3.3.2 for more details. The circuit diagram of a Cooper pair box is shown in figure 3.2. If the Cooper pair box is small enough, the electrostatic charging energy is so large that the tunneling of electrons can be controlled on the level of a single Cooper pair, even though there is a large number of Cooper pairs on the island. This pair tunneling on and off the island constitutes the dipole emitter in this case. [10, 11]

The Hamiltonian describing the superconducting island is in the Cooper pair number basis $\{|N\rangle\}$ [12]

$$H_Q = 4E_C \sum_N (N - N_g)^2 \, |N\rangle\langle N| - \frac{E_J}{2} \sum_N (|N+1\rangle\langle N| + |N\rangle\langle N+1|), \quad (3.11)$$

where

$$E_C = \frac{e^2}{2C_\Sigma} \quad (3.12a)$$

$$N_g = \frac{C_g V_g}{2e}, \quad (3.12b)$$

with $C_\Sigma = C_g + C_J$ being the total box capacitance and e the charge of an electron. E_J, C_J, C_g and V_g are the Josephson energy, Josephson capac-

itance, gate capacitance and gate voltage, respectively, as shown in figure 3.2. When the number of Cooper pairs on the island is restricted to at most one, that is, $N = 0, 1$, the Hamiltonian is reduced to

$$H_Q = -2E_C(1 - 2N_g)\sigma_z - \frac{E_J}{2}\sigma_x, \tag{3.13}$$

where $\sigma_z = |0\rangle\langle 0| - |1\rangle\langle 1|$ and $\sigma_x = |1\rangle\langle 0| + |0\rangle\langle 1|$. For a superconducting island inside a microwave resonator, the gate voltage consists of a DC part V_g^{DC} and a quantum part v,

$$V_g = V_g^{\mathrm{DC}} + v. \tag{3.14}$$

As is shown in Ref. [12], if the Cooper pair box qubit is placed in the center of the resonator, the quantum part is given by

$$v = V_{\mathrm{rms}}^0(a^\dagger + a), \tag{3.15}$$

where $V_{\mathrm{rms}}^0 = \sqrt{\hbar\omega_r/Lc}$, ω_r is the cavity frequency, L is the length of the transmission line and c is the capacitance per unit length. Taking V_g^{DC} and v into account in (3.13), we obtain

$$\begin{aligned} H_Q = H_{\mathrm{CPB}} + H_{\mathrm{int}} = &- 2E_C(1 - 2N_g^{\mathrm{DC}})\sigma_z - \frac{E_J}{2}\sigma_x \\ &- e\frac{C_g}{C_\Sigma}\sqrt{\frac{\hbar\omega_r}{Lc}}(a^\dagger + a)(1 - 2N_g^{\mathrm{DC}} - \sigma_z), \end{aligned} \tag{3.16}$$

where $N_g^{\mathrm{DC}} = C_g V_g^{\mathrm{DC}}/2e$. The first two terms of (3.16) are the bare Cooper pair box Hamiltonian and the last term describes the interaction with the microwave field. Working in the eigenbasis of H_{CPB} and adding the term describing the free microwave cavity field, the complete Hamiltonian of the interacting qubit and resonator takes the form

$$\begin{aligned} H = \hbar\omega_r a^\dagger a + \frac{\hbar\Omega}{2}\sigma_z - e\frac{C_g}{C_\Sigma}\sqrt{\frac{\hbar\omega_r}{Lc}}(a^\dagger + a) \\ \times[1 - 2N_g^{\mathrm{DC}} - \cos(\theta)\sigma_z + \sin(\theta)\sigma_x], \end{aligned} \tag{3.17}$$

where

$$\theta = \arctan\left(\frac{E_J}{4E_C(1 - 2N_g^{\mathrm{DC}})}\right) \tag{3.18}$$

is the mixing angle and

$$\hbar\Omega = \sqrt{E_J^2 + [4E_C(1 - 2N_g^{\mathrm{DC}})]^2} \tag{3.19}$$

is the energy splitting of the qubit. At the charge degeneracy point where $N_g^{\mathrm{DC}} = 1/2$ and $\theta = \pi/2$, the Hamiltonian becomes

$$H = \hbar\omega_r a^\dagger a + \frac{\hbar\Omega}{2}\sigma_z - \hbar g(a^\dagger + a)\sigma_x, \tag{3.20}$$

where the coupling is

$$\hbar g = e\frac{C_g}{C_\Sigma}\sqrt{\frac{\hbar\omega_r}{Lc}}. \tag{3.21}$$

This is equivalent to the Rabi model of cavity QED. In the rotating wave approximation, equation (3.20) is reduced to the Jaynes-Cummings form equivalent to the Hamiltonian (3.1):

$$H = \hbar\omega_r a^\dagger a + \frac{\hbar\Omega}{2}\sigma_z - \hbar g(\sigma_+ a + \sigma_- a^\dagger). \tag{3.22}$$

We therefore see that the circuit QED setup can be used as an analog to cavity QED, with the Cooper pair box acting as an artificial atom. [11, 12]

3.2 Ion Trap

Let us now justify the Hamiltonian of a trapped and laser-irradiated ion [11, 23], in which the quantized center-of-mass motion of the ion is coupled to its electronic states via the laser, and external lasers drive a two-level transition between the ground and excited electronic states.

It follows from Laplace's equation that it is not possible to trap an ion in three dimensions with an electrostatic potential. That is why, in an ion trap, the position of the ion is restricted using a time periodic potential. One such potential [23] of approximately quadrupolar shape may be written as

$$\Phi(x,y,z,t) = \frac{U}{2}(\alpha x^2 + \beta y^2 + \gamma z^2) + \frac{\widetilde{U}}{2}\cos(\omega_{\mathrm{rf}} t)(\alpha' x^2 + \beta' y^2 + \gamma' z^2), \tag{3.23}$$

where ω_{rf} is the frequency of the time-dependent potential, U and $\widetilde{U}$ are amplitudes and α, β, γ, α', β', γ' are geometric factors. Because this potential has to satisfy the Laplace equation $\nabla^2\Phi = 0$ at every point in time, we find the conditions

$$\alpha + \beta + \gamma = 0 \tag{3.24a}$$

$$\alpha' + \beta' + \gamma' = 0. \tag{3.24b}$$

From these conditions we can see what we already stated, that no local three-dimensional minimum can be generated. The potential can only trap ions in a dynamical way.

We will first show that the classical center-of-mass motion of the ion is approximately harmonic. Consider the classical equations of motion of a particle with mass m and charge $Z|e|$ in a potential of the form (3.23). They are decoupled in the spatial coordinates, so each dimension can be considered separately. We will only discuss motion in the x-direction, recognizing that the other directions are treated analogously. The equation of motion is then

$$\ddot{x} = -\frac{Z|e|}{m}\frac{\partial \Phi}{\partial x} = -\frac{Z|e|}{m}[U\alpha + \widetilde{U}\cos(\omega_{\mathrm{rf}}t)\alpha']x. \tag{3.25}$$

By making the substitutions

$$\xi = \frac{\omega_{\mathrm{rf}}t}{2} \tag{3.26a}$$

$$a_x = \frac{4Z|e|U\alpha}{m\omega_{\mathrm{rf}}^2} \tag{3.26b}$$

$$q_x = \frac{2Z|e|\widetilde{U}\alpha'}{m\omega_{\mathrm{rf}}^2}, \tag{3.26c}$$

the equation of motion is transformed into the standard form of the Mathieu equation,

$$\frac{\mathrm{d}^2x}{\mathrm{d}\xi^2} + [a_x - 2q_x\cos(2\xi)]x = 0. \tag{3.27}$$

The Mathieu equation has a solution that follows from the Floquet theorem,

$$x(\xi) = Ae^{i\beta_x\xi}\sum_{n=-\infty}^{\infty} C_{2n}e^{i2n\xi} + Be^{-i\beta_x\xi}\sum_{n=-\infty}^{\infty} C_{2n}e^{-i2n\xi}, \tag{3.28}$$

where the real-valued characteristic exponent β_x and the coefficients C_{2n} are functions of a_x and q_x. A and B are constants that can be used to satisfy boundary conditions or normalize a solution. Substituting (3.28) into (3.27) yields a recursion relation

$$C_{2n+2} - D_{2n}C_{2n} + C_{2n-2} = 0, \tag{3.29}$$

where

$$D_{2n} = [a_x - (2n + \beta_x)^2]/q_x. \tag{3.30}$$

From this we can obtain continued fraction expressions for the coefficients C_{2n},

$$C_{2n+2} = \frac{C_{2n}}{D_{2n} - \frac{1}{D_{2n+2} - \frac{1}{\cdots}}} \tag{3.31a}$$

$$C_{2n} = \frac{C_{2n-2}}{D_{2n} - \frac{1}{D_{2n-2} - \frac{1}{\cdots}}}, \tag{3.31b}$$

and for β_x^2,

$$\beta_x^2 = a_x - q_x \left(\frac{1}{D_0 - \frac{1}{D_2 - \frac{1}{\cdots}}} + \frac{1}{D_0 - \frac{1}{D_{-2} - \frac{1}{\cdots}}} \right). \tag{3.32}$$

The contributions of higher orders in the continued fractions (3.31) and (3.32) fall off rapidly for typical values of a_x and q_x. Numerical values for β_x^2 and the coefficients can therefore be gained by truncating the expressions once the desired accuracy has been reached. In the case of $|a_x|, |q_x| \ll 1$, the lowest order approximation for the ion trajectory is found by assuming $C_{\pm 4} \approx 0$. With the initial condition $A = B$ we then get

$$\beta_x \approx \sqrt{a_x + q_x^2/2} \tag{3.33a}$$

$$x(t) \approx 2AC_0 \cos\left(\beta_x \frac{\omega_{\mathrm{rf}}}{2} t\right) \left[1 - \frac{q_x}{2} \cos(\omega_{\mathrm{rf}} t)\right]. \tag{3.33b}$$

The motion of the ion consists of two parts: harmonic oscillation with the secular frequency

$$\nu = (a_x + q_x^2/2)^{1/2} \omega_{\mathrm{rf}}/2 \ll \omega_{\mathrm{rf}} \tag{3.34}$$

and so-called micromotion at frequency ω_{rf}. The latter oscillations are much faster and smaller than the secular motion, so we neglect them.

We have now shown that the classical motion of the ion in a potential of the form (3.23) is harmonic as a first approximation. Quantum mechanical treatment yields the same result, as is shown by Leibfried et al. [23]. We will proceed assuming that this is so.

The ion trap Hamiltonian consists of three parts,

$$H = H_m + H_q + H_{\mathrm{int}}, \tag{3.35}$$

where H_m describes the center-of-mass motion, H_q is the Hamiltonian of the bare two-level ion and H_{int} is the coupling. Because the ion vibrates harmonically in the trap potential,

$$H_m = \hbar \nu a^\dagger a, \tag{3.36}$$

where ν is the vibrational frequency (3.34). We have neglected the zero-point energy, as usual. From section 3.1.1, we know the two-level Hamiltonian to be

$$H_q = \frac{\hbar\omega_0}{2}\sigma_z, \tag{3.37}$$

where ω_0 is the frequency of the electronic transition. Equation (3.10) gives an alternate form for this term. The coupling term in the rotating wave approximation is given by Vogel et al. [24] to be

$$H_{\text{int}}(t) = \lambda E^{(-)}(t)g(x)\sigma_- + \lambda[E^{(-)}(t)]^\dagger[g(x)]^\dagger\sigma_+, \tag{3.38}$$

where λ is the coupling matrix element and $E^{(-)}(t) = E_0 e^{i\omega_l t}$ is the negative frequency part of the laser electric field with amplitude E_0 and frequency ω_l. The operator-valued function $g(x)$ describes the mode structure of the laser field, and is for a standing wave

$$g(x) = \cos\Big(\frac{\omega_l}{c}x + \phi\Big), \tag{3.39}$$

where ϕ defines the position of the wave with respect to the trap potential and c is the speed of light. The operator x is

$$x = \frac{\eta c}{\omega_l}(a^\dagger + a), \tag{3.40}$$

η being the Lamb-Dicke parameter. Assuming the time-dependence has minor effect, as is usually the case, we set $H_{\text{int}} = H_{\text{int}}(0)$ and, because $[g(x)]^\dagger = g(x)$,

$$\begin{aligned} H_{\text{int}} &= 2\lambda E_0 \cos\Big(\eta(a^\dagger + a) + \phi\Big)(\sigma_- + \sigma_+) \\ &= 2\lambda E_0 \cos\Big(\eta(a^\dagger + a) + \phi\Big)\sigma_x. \end{aligned} \tag{3.41}$$

Defining $\hbar g = 2\lambda E_0$, the ion trap Hamiltonian becomes

$$H = \hbar\nu a^\dagger a + \frac{\hbar\omega_0}{2}\sigma_z + \hbar g \cos\Big(\eta(a^\dagger + a) + \phi\Big)\sigma_x. \tag{3.42}$$

If $\eta \ll 1$ (the Lamb-Dicke regime), the coupling can be linearized and the Hamiltonian reduced to the linear Rabi or Jaynes-Cummings form. However, later on we will be interested in the case in which this does not hold. [11, 23, 24]

3.3 Artificial Trapped Ion

We wish to construct an artificial trapped ion using superconducting circuits. We will show that a single Cooper pair transistor coupled to an LC resonator has the desired Hamiltonian. We will go through the principles of the circuit analysis following the discussion by Tuorila [25]. But first we will review Josephson junctions in some more detail and introduce some relevant concepts of quantum network theory, which was founded by Yurke and Denker [26], and generalized by Devoret [27].

3.3.1 Quantum Network Theory

By using quantum network theory, an electric circuit can be described with the Hamiltonian formalism familiar from classical dynamics. The first step is therefore defining a coordinate system.

A circuit consists of branches. To each branch b is associated a potential difference V_b and a current I_b. Using these, we define the branch flux $\Phi_b(t)$ and charge $Q_b(t)$ as

$$\Phi_b(t) = \int_{-\infty}^{t} V_b(t')dt' \tag{3.43a}$$

$$Q_b(t) = \int_{-\infty}^{t} I_b(t')dt'. \tag{3.43b}$$

The integration is started at a time when the circuit was at rest and no currents or voltages were present. The energy stored in branch b is given by

$$E_b(t) = \int_{-\infty}^{t} V_b(t')I_b(t')dt'. \tag{3.44}$$

From equations (3.43) we get the relations

$$V_b(t) = \dot{\Phi}_b(t) \tag{3.45a}$$

$$I_b(t) = \dot{Q}_b(t). \tag{3.45b}$$

Let us calculate the energies of a capacitor and an inductor, which are basic elements of the SCPT-LC circuit. A capacitor with capacitance C is described by the relation $Q_b = CV_b$, giving

$$\begin{aligned} E_C &= \int_{-\infty}^{t} V_b(t')I_b(t')dt' = \int_{-\infty}^{t} \frac{Q_b}{C}\frac{\mathrm{d}Q_b}{\mathrm{d}t'}dt' = \int_0^{Q_C} \frac{Q_b}{C}dQ_b \\ &= \frac{Q_C^2}{2C} = \frac{1}{2}C\dot{\Phi}_C^2. \end{aligned} \tag{3.46}$$

For an inductor with inductance L, we have $\Phi_b = LI_b$, which results in

$$\begin{aligned} E_L &= \int_{-\infty}^{t} V_b(t')I_b(t')dt' = \int_{-\infty}^{t} \frac{\Phi_b}{L}\frac{\mathrm{d}\Phi_b}{\mathrm{d}t'}dt' = \int_0^{\Phi_L} \frac{\Phi_b}{L}d\Phi_b \\ &= \frac{\Phi_L^2}{2L}. \end{aligned} \tag{3.47}$$

In constructing the Lagrangian, which is defined as the difference between the kinetic energy T and the potential energy U,

$$\mathcal{L} = T - U, \tag{3.48}$$

we can associate terms depending on $\dot{\Phi}$ as kinetic and terms depending on Φ as potential.

The branch variables are constrained by the Kirchhoff rules, which state that the potential differences around any closed loop and the currents arriving at each node must sum to zero. Stated in terms of the branch fluxes and charges these are

$$\sum_{\text{all } b \text{ around loop}} \Phi_b = \tilde{\Phi}_l \tag{3.49a}$$

$$\sum_{\text{all } b \text{ arriving at node}} Q_b = \tilde{Q}_n, \tag{3.49b}$$

where $\tilde{\Phi}_l$ and $\tilde{Q}_n$ are constants. If we choose the branch fluxes as canonical coordinates and take the constraints (3.49) into account, we end up with a set of N independent coordinates Φ_i. For each coordinate, a canonical momentum can now be defined as

$$q_i = \frac{\partial \mathcal{L}}{\partial \dot{\Phi}_i}. \tag{3.50}$$

Note that this is not the same as the spatial coordinate in section 2.1. The classical Hamiltonian of the circuit is then

$$\mathcal{H} = \sum_i \dot{\Phi}_i q_i - \mathcal{L}. \tag{3.51}$$

Quantization is accomplished by replacing the canonically conjugated variables Φ and q with corresponding operators satisfying the commutation relation

$$[\Phi, q] = i\hbar \tag{3.52}$$

in direct analogy with the position and momentum operators of section 2.1. [10, 25, 27]

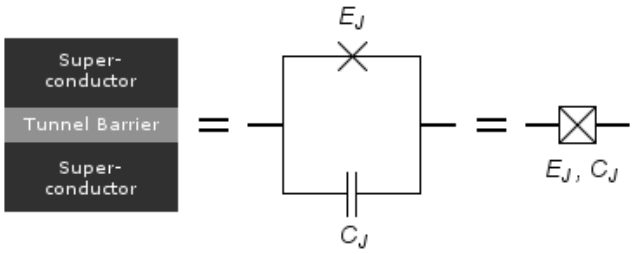

Figure 3.3: A sketch and a circuit diagram of a Josephson junction. The two superconductors are linked by a tunneling barrier, through which Cooper pairs may tunnel. In addition to the inductive energy characterized by E_J, a real Josephson junction also contains capacitive energy characterized by C_J when attached to a voltage source.

3.3.2 Josephson Junction

In low temperatures, many materials lose their electric resistivity, and it is said they become superconducting. The phenomenon is explained by the BCS-theory. In this theory, the spin-1/2 electrons (fermions) can overcome the Coulomb repulsion in low temperatures and form Cooper pairs that behave like bosons. The attraction originates from the electron-phonon interactions between the electrons and the lattice. The Pauli exclusion principle states that no two identical fermions may occupy the same quantum state; bosons have no such limitation. Therefore, in low temperatures the bosonic Cooper pairs can form a so-called condensate at the ground state of the superconductor. With the Cooper pairs occupying the same state, the state of the entire superconductor can be described by a single wave function.

Electrical resistance in a metal is caused by interactions between the electric current and the vibrations or impurities of the lattice. There is an energy gap between the ground state of the Cooper pair condensate and the excited state, which implies the necessary quantum transitions will not always be possible. This means the electron transport can occur without resistance.

A Josephson junction consists of two superconductors separated by a tunneling barrier, which can be an insulating layer (figure 3.3). If the barrier is thin enough, the probability for Cooper pairs to tunnel through it becomes sufficiently large. The resulting Cooper pair current can be written as

$$I = I_c \sin \phi, \tag{3.53}$$

where the critical current I_c depends of the material and ϕ is the difference in phase factor between the Ginzburg-Landau complex order parameters of the condensates. Even in the absence of voltages, there is a supercurrent across the junction that depends sinusoidally on the phase difference. This is called the the dc Josephson effect. If a potential difference V is applied across the junction, the phase ϕ can be written as

$$\phi = \frac{2\pi\Phi_J}{\Phi_0}, \tag{3.54}$$

where Φ_J is the branch flux and $\Phi_0 = h/2e$ is the superconducting flux quantum. This relation gives the ac Josephson effect, which says that at a constant potential difference $V \neq 0$ there is an alternating current across the junction, since $\Phi_J(t) = Vt + \text{constant}$.

We can now calculate the inductive energy of the Josephson junction using equation (3.44):

$$\begin{aligned} U_J &= \int_{-\infty}^{t} V_b(t')I_b(t')dt' = \int_{-\infty}^{t} I_c \sin\frac{2\pi\Phi_b}{\Phi_0}\frac{\mathrm{d}\Phi_b}{\mathrm{d}t'}dt' \\ &= \int_0^{\Phi_J} I_c \sin\frac{2\pi\Phi_b}{\Phi_0}d\Phi_b = -E_J\cos\frac{2\pi\Phi_J}{\Phi_0}, \end{aligned} \tag{3.55}$$

where $E_J = I_c\Phi_0/2\pi$. A real Josephson junction also stores capacitive energy,

$$E_{J,C} = \frac{Q_J^2}{2C_J} = \frac{1}{2}C_J\dot{\Phi}_J^2, \tag{3.56}$$

in addition to the inductive energy (3.55). [10, 25]

3.3.3 SCPT Coupled to LC Resonator

The circuit diagram of a single Cooper pair transistor coupled to an LC resonator is shown in figure 3.4. The capacitive energies are associated as kinetic, giving the kinetic energy

$$T = \frac{1}{2}C_1\dot{\Phi}_1^2 + \frac{1}{2}C_2\dot{\Phi}_2^2 + \frac{1}{2}C_3\dot{\Phi}_3^2 + \frac{1}{2}C_4\dot{\Phi}_4^2 + \frac{1}{2}C_g\dot{\Phi}_g^2. \tag{3.57}$$

Conversely, inductive and Josephson energies are thought of as potential, which gives the potential energy

$$U = -E_{J1}\cos\frac{2\pi\Phi_1}{\Phi_0} - E_{J2}\cos\frac{2\pi\Phi_2}{\Phi_0} + \frac{1}{2}LI^2 + \frac{1}{2}L_{\text{ext}}I_{\text{ext}}^2 + MII_{\text{ext}}, \tag{3.58}$$

where $\Phi = \Phi_5$ has been chosen as the flux coordinate. The auxiliary coil, which provides flux control to the qubit, induces an external flux $\Phi_{\text{ext}} =$

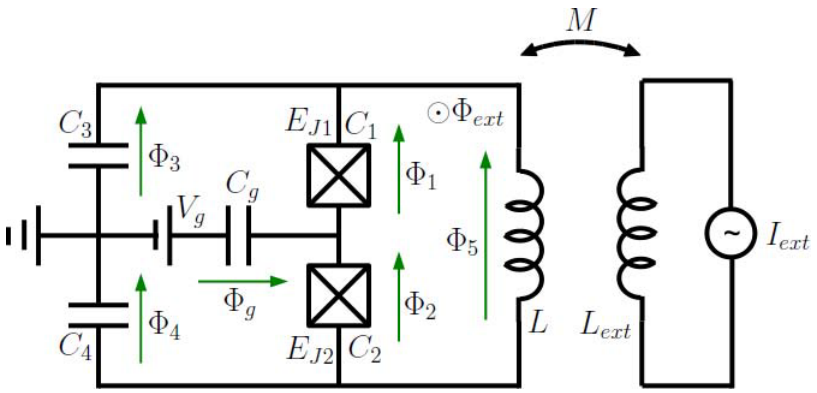

Figure 3.4: Circuit diagram of an SCPT coupled to an LC resonator. The gate voltage V_g, gate capacitance C_g and the Josephson junctions make up the SCPT. The external inductance loop on the right allows flux control of the circuit through the mutual inductance M, which induces the external flux $\Phi_{\text{ext}} = MI_{\text{ext}}$. From [25].

MI_{ext} to the system through the mutual inductance M. The last term in equation (3.58) describes the energy of this interaction.

Following the rules of quantum network theory, we get the constraints

$$\Phi + \Phi_{\text{ext}} = \Phi_1 + \Phi_2 = \Phi_3 + \Phi_4 \tag{3.59a}$$

$$\dot{\Phi}_g = \dot{\Phi}_2 - \dot{\Phi}_4 - V_g. \tag{3.59b}$$

We then make the variable changes

$$\Theta = \frac{\Phi_2 - \Phi_1}{2} \tag{3.60a}$$

$$\Theta_1 = \frac{\Phi_4 - \Phi_3}{2}, \tag{3.60b}$$

giving

$$\Phi_1 = \frac{\Phi + \Phi_{\text{ext}}}{2} - \Theta \tag{3.61a}$$

$$\Phi_2 = \frac{\Phi + \Phi_{\text{ext}}}{2} + \Theta \tag{3.61b}$$

$$\Phi_3 = \frac{\Phi + \Phi_{\text{ext}}}{2} - \Theta_1 \tag{3.61c}$$

$$\Phi_4 = \frac{\Phi + \Phi_{\text{ext}}}{2} + \Theta_1. \tag{3.61d}$$

The Lagrangian $\mathcal{L} = T - U$ now has three independent variables that have the canonical momenta $q = \frac{\partial \mathcal{L}}{\partial \dot{\Phi}}$, $Q = \frac{\partial \mathcal{L}}{\partial \dot{\Theta}}$ and $p = \frac{\partial \mathcal{L}}{\partial \dot{\Theta}_1}$. From here, it

is a matter of straightforward if lengthy algebra to calculate the classical Hamiltonian

$$\begin{aligned}\mathcal{H} &= \dot{\Phi}q + \dot{\Theta}Q + \dot{\Theta}_1 p - \mathcal{L} \\ &= \frac{q^2}{2C} + \frac{\Phi^2}{2L} - q\dot{\Phi}_{\text{ext}} \\ &+ \frac{(Q-Q_0)^2}{2C_\Sigma} - E_{J0}\cos\frac{\pi(\Phi+\Phi_{\text{ext}})}{\Phi_0}\cos\frac{2\pi\Theta}{\Phi_0} - dE_{J0}\sin\frac{\pi(\Phi+\Phi_{\text{ext}})}{\Phi_0}\sin\frac{2\pi\Theta}{\Phi_0},\end{aligned} \tag{3.62}$$

when $C_g \ll C_1, C_3$. The system does not explicitly depend on Θ_1, so the corresponding canonical momentum is a constant of motion. We have therefore set $p = Q_0 = C_g V_g$. We have assumed capacitive symmetry $C_1 = C_2$ and $C_3 = C_4$, and used the notations $C = (C_1 + C_3)/2$, $C_\Sigma = C_1 + C_2 + C_g$ and $E_{J0} = E_{J1} + E_{J2}$. We have also defined the so-called asymmetry parameter $d = (E_{J1} - E_{J2})/E_{J0}$. The first three terms in equation (3.62),

$$\mathcal{H}_o = \frac{q^2}{2C} + \frac{\Phi^2}{2L} - q\dot{\Phi}_{\text{ext}}, \tag{3.63}$$

have a straightforward interpretation. They describe a driven LC oscillator with the driving term caused by the external flux. The remaining Hamiltonian describes the SCPT,

$$\begin{aligned}\mathcal{H}_{\text{SCPT}} =& \frac{(Q-Q_0)^2}{2C_\Sigma} \\ &- E_{J0}\cos\frac{\pi(\Phi+\Phi_{\text{ext}})}{\Phi_0}\cos\frac{2\pi\Theta}{\Phi_0} - dE_{J0}\sin\frac{\pi(\Phi+\Phi_{\text{ext}})}{\Phi_0}\sin\frac{2\pi\Theta}{\Phi_0}.\end{aligned} \tag{3.64}$$

The Hamiltonian (3.62) is quantized by replacing q, Φ, Q and Θ with the corresponding operators, for which $[\Phi, q] = i\hbar$ and $[\Theta, Q] = i\hbar$. The SCPT Hamiltonian can be expressed in the charge basis $|N\rangle$,

$$H_{\text{SCPT}} = \sum_N \left[4E_C(N-N_0)^2 |N\rangle - \frac{E_J(\Phi)}{2}\Big(e^{i\phi}|N+1\rangle + e^{-i\phi}|N-1\rangle\Big)\right]\langle N|, \tag{3.65}$$

where N is the number of Cooper pairs on the island separated by the gate capacitance and the Josephson junctions, the charging energy $E_C = e^2/2C_\Sigma$ and the effective Josephson energy

$$E_J(\Phi) = E_{J0}\sqrt{\cos^2\frac{\pi\Phi}{\Phi_0} + d^2\sin^2\frac{\pi\Phi}{\Phi_0}}. \tag{3.66}$$

In addition, $N_g = C_g V_g/2e$ and $\tan\phi = -d\tan\frac{\pi\Phi}{\Phi_0}$. In the charge limit $E_{J0} \ll E_C$, the energy difference between the two lowest states $|0\rangle$ and $|1\rangle$ is much smaller than the energy differences between other states, so the Hamiltonian can be truncated to include only them. Making this two-state approximation and separating the static flux Φ_b from the external flux $\Phi_{\text{ext}} = \Phi_b + \Phi_L(t)$ leads to the Hamiltonian

$$\begin{aligned} H = {} & \frac{q^2}{2C} + \frac{\Phi^2}{2L} - q\dot{\Phi}_L(t) + \frac{E_{el}}{2}\sigma_z \\ & - \frac{1}{2}E_{J0}\Bigg[\cos\frac{\pi(\Phi+\Phi_L(t))}{\Phi_0}\Big(\cos\frac{\pi\Phi_b}{\Phi_0}\sigma_x - d\sin\frac{\pi\Phi_b}{\Phi_0}\sigma_y\Big) \\ & - \sin\frac{\pi(\Phi+\Phi_L(t))}{\Phi_0}\Big(\sin\frac{\pi\Phi_b}{\Phi_0}\sigma_x + d\cos\frac{\pi\Phi_b}{\Phi_0}\sigma_y\Big)\Bigg], \end{aligned} \tag{3.67}$$

where $E_{el} = 4E_C(1-2N_g)$. [25]

If we assume Φ_{ext} is time-independent, the driving term disappears and we have

$$H_o = \frac{q^2}{2C} + \frac{\Phi^2}{2L}. \tag{3.68}$$

Next we will assume the circuit is symmetric, $d = 0$, so the Hamiltonian is reduced to the form

$$\begin{aligned} H = {} & \frac{q^2}{2C} + \frac{\Phi^2}{2L} + \frac{E_{el}}{2}\sigma_z \\ & - \frac{1}{2}E_{J0}\Bigg[\cos\frac{\pi(\Phi+\Phi_{\text{ext}}-\Phi_b)}{\Phi_0}\cos\frac{\pi\Phi_b}{\Phi_0}\sigma_x \\ & - \sin\frac{\pi(\Phi+\Phi_{\text{ext}}-\Phi_b)}{\Phi_0}\sin\frac{\pi\Phi_b}{\Phi_0}\sigma_x\Bigg], \end{aligned} \tag{3.69}$$

Now we take $\Phi_b = \frac{1}{2}\Phi_0$ and get

$$\begin{aligned} H = {} & \frac{q^2}{2C} + \frac{\Phi^2}{2L} + \frac{E_{el}}{2}\sigma_z \\ & + \frac{1}{2}E_{J0}\sin\Big(\frac{\pi(\Phi+\Phi_{\text{ext}})}{\Phi_0} - \frac{\pi}{2}\Big)\sigma_x \\ = {} & \frac{q^2}{2C} + \frac{\Phi^2}{2L} + \frac{E_{el}}{2}\sigma_z - \frac{E_{J0}}{2}\cos\Big(\frac{\pi\Phi}{\Phi_0} + \frac{2e\pi\Phi_{\text{ext}}}{h}\Big)\sigma_x. \end{aligned} \tag{3.70}$$

Let us define annihilation and creation operators for the LC oscillator analogously to those of the harmonic oscillator:

$$a = \frac{1}{\sqrt{2\hbar}}\Big(\sqrt{C\omega_c}\Phi + i\frac{q}{\sqrt{C\omega_c}}\Big) \tag{3.71a}$$

$$a^\dagger = \frac{1}{\sqrt{2\hbar}}\Big(\sqrt{C\omega_c}\Phi - i\frac{q}{\sqrt{C\omega_c}}\Big), \tag{3.71b}$$

where $\omega_c = 1/\sqrt{LC}$ is the oscillator frequency. By inverting these and substituting them into equation (3.70) we obtain

$$H = \hbar\omega_c a^\dagger a + \frac{\hbar\omega_0}{2}\sigma_z - \hbar g \cos\Big(\eta(a^\dagger + a) + \phi_{\text{ext}}\Big)\sigma_x, \tag{3.72}$$

where $\hbar\omega_0 = E_{el} = 4E_C(1 - 2N_g)$, $\hbar g = E_{J0}/2$, $\eta = \sqrt{e^2\omega_c L/(2\hbar)}$, $\phi_{\text{ext}} = e\Phi_{\text{ext}}/\hbar$ and the zero-point energy of the oscillator has, as usual, been neglected. This is of the same form as the real ion trap Hamiltonian (3.42) apart from a phase shift at the interaction term. Thus we can call the SCPT-LC circuit an artificial trapped ion.

Again, with small values of the Lamb-Dicke parameter η the coupling can be linearized. However, it is possible to have such large values of η that the nonlinearities cannot be neglected [28]. This is what we will assume in the future.

3.3.4 Coupled Artificial Trapped Ions

Two artificial trapped ions can be coupled through the mutual inductance of the inductance loops. Consider inductance loops L_1 and L_2 interacting via mutual inductance M. Loop 2 induces the flux $-MI_2$ in loop 1 and loop 1 the flux $-MI_1$ in loop 2, I_1 and I_2 being the currents flowing in the inductors [29]. The energy of the system is then

$$\begin{aligned} E_L^{\text{tot}} &= \int_{-\infty}^{t} V_1(t')I_1(t')dt' + \int_{-\infty}^{t} V_2(t')I_2(t')dt' \\ &= \int_{-\infty}^{t} \left[I_1\frac{\mathrm{d}\Phi_1}{\mathrm{d}t'} - MI_1\frac{\mathrm{d}I_2}{\mathrm{d}t'} + I_2\frac{\mathrm{d}\Phi_2}{\mathrm{d}t'} - MI_2\frac{\mathrm{d}I_1}{\mathrm{d}t'}\right] dt' \\ &= E_{L_1} + E_{L_2} - M\int_{-\infty}^{t} \frac{\mathrm{d}I_1 I_2}{\mathrm{d}t'}dt' \\ &= E_{L_1} + E_{L_2} - MI_1(t)I_2(t). \end{aligned} \tag{3.73}$$

The classical interaction energy is therefore $E_{\text{int}} = -MI_1I_2 = -\frac{M}{L_1L_2}\Phi_1\Phi_2$. We construct the quantized interaction Hamiltonian by replacing the flux coordinates with the corresponding operators. Using definitions (3.71), the Hamiltonian can be written in the form

$$H_{\text{int}} = -\frac{M}{L_1L_2}\Phi_{\text{zp}}^{(1)}\Phi_{\text{zp}}^{(2)}(a_1 + a_1^\dagger)(a_2 + a_2^\dagger) = -\hbar J(a_1 + a_1^\dagger)(a_2 + a_2^\dagger), \tag{3.74}$$

where $\Phi_{\text{zp}}^{(1,2)} = \sqrt{\hbar L_{1,2}\omega_c^{1,2}/2}$ and the hopping frequency is defined

$$J = \frac{M}{\hbar L_1 L_2}\Phi_{\text{zp}}^{(1)}\Phi_{\text{zp}}^{(2)}. \tag{3.75}$$

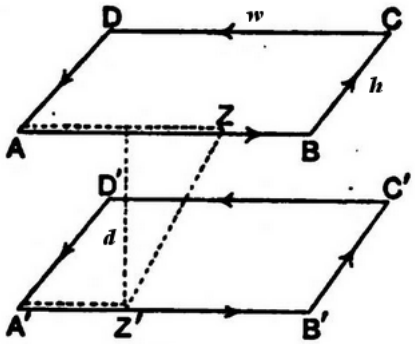

Figure 3.5: Sketch of two identical rectangular inductance loops. From [30].

The mutual inductance can be calculated using the Neumann formula,

$$M = \frac{\mu_0}{4\pi} \oint_{C_1} \oint_{C_2} \frac{dl_1 \cdot dl_2}{r}, \tag{3.76}$$

where the integration is performed over closed contours determined by the inductance loops and r is the distance between line elements. Let us consider two identical rectangular loops with width w and height h a distance d apart as in figure 3.5. The integral vanishes for the pairs of sides that are perpendicular. For pairs of parallel sides the dot product is plus unity for corresponding sides and minus unity for opposite sides. For the sides AB, $A'B'$ the integral is

$$\int_0^w \int_0^w \frac{dzdz'}{\sqrt{d^2 + (z' - z)^2}} = \int_0^w \ln \frac{\sqrt{d^2 + (w - z)^2} + w - z}{\sqrt{d^2 + z^2} - z} dz. \tag{3.77}$$

The second integration can be performed by assigning the quantity inside the logarithm as the new variable and integrating by parts. The result is

$$2\left[d - \sqrt{d^2 + w^2} + w \ln \frac{w + \sqrt{d^2 + w^2}}{d}\right]. \tag{3.78}$$

The integral for the pair of sides AB, $C'D'$ is found by substituting $\sqrt{d^2 + h^2}$ for d and changing the sign, resulting in

$$-2\left[\sqrt{d^2 + h^2} - \sqrt{d^2 + h^2 + w^2} + w \ln \frac{w + \sqrt{d^2 + h^2 + w^2}}{\sqrt{d^2 + h^2}}\right]. \tag{3.79}$$

The parts for the remaining sides BC, $B'C'$ and BC, $D'A'$ can be obtained from these by interchanging w and h. By adding these four parts together we

will have considered half of the two loops. We get the whole inductance by multiplying with two, as the calculation of the other half follows an identical process. The final mutual inductance of the rectangular loops is then

$$\begin{aligned} M = \frac{\mu_0}{\pi}\Bigg[& w \ln\left(\frac{w+\sqrt{d^2+w^2}}{w+\sqrt{d^2+h^2+w^2}}\frac{\sqrt{d^2+h^2}}{d}\right) \\ & + h\ln\left(\frac{h+\sqrt{d^2+h^2}}{h+\sqrt{d^2+h^2+w^2}}\frac{\sqrt{d^2+w^2}}{d}\right)\Bigg] \\ & + \frac{2\mu_0}{\pi}\Big[\sqrt{d^2+h^2+w^2} - \sqrt{d^2+w^2} - \sqrt{d^2+h^2} + d\Big]. \end{aligned} \tag{3.80}$$

[30]

Utilizing the experimentally achievable values used by Tuorila et al. [31] in experiments with a circuit of the kind we are studying, $w = 50$ μm and $h = 125$ μm, and $d = 10$ μm, we obtain

$$M \approx 93 \text{ pH}. \tag{3.81}$$

From this we can easily calculate the hopping frequency by using the parameters $L = 410$ pH and $\omega_c/(2\pi) = 3.5$ GHz [31]:

$$J/(2\pi) \approx 0.4 \text{ GHz}. \tag{3.82}$$

This gives us a ball-park estimate for the strength of the coupling between the artificial trapped ions:

$$\frac{J}{\omega_c} \sim 0.1. \tag{3.83}$$

Therefore, the above scheme appears feasible with current technology.

Chapter 4

Rabi-Hubbard Model

Bosonic and fermionic lattices realized with, for instance, ultracold atoms have long been used to simulate many-body quantum systems. Recently, increased control over light-matter interactions at the quantum level has led to cavity QED systems being explored as the basic building blocks of such lattices. The interplay between photon blockade and inter-cavity photon tunneling in cavity QED lattices leads to phenomenology similar to Hubbard models of massive bosons.

Circuit QED provides an especially promising experimental platform for realizing Rabi or Jaynes-Cummings lattices. In a circuit QED lattice, photons can hop between transmission line resonators and locally interact with a qubit. The qubit energy can be tuned by an external magnetic flux.

Novel quantum phenomena are expected to emerge in CQED systems coupled to form a lattice, such as phase transitions of light between Mott-like insulating and superfluid phases induced by the competition between photon blockade and inter-cavity tunneling. These systems have potential as dissipative quantum simulators that provide full access to individual sites through continuous weak measurements. Quantum simulation is a fast-growing field in which a simple or controllable quantum system is used to study another, more complex or less accessible quantum system [32, 33]. It promises to have numerous applications in not only condensed matter physics, but also high-energy physics, nuclear and atomic physics, quantum chemistry and cosmology, among others. CQED lattices have also been proposed to have potential in realizing artificial gauge fields and quantum Hall fluids of light [1, 2].

At a certain critical value of the cavity-cavity coupling strength, a lattice of coupled Rabi systems is driven across a Z_2 parity symmetry-breaking

quantum phase transition between a Rabi insulator and a delocalized superradiant phase, which is our main object of interest. [4–6]

4.1 CQED Lattice

We will use the Rabi model (3.4) or correspondingly (3.20) for the CQED systems rather than the approximated Jaynes-Cummings model. The single-site Hamiltonian at lattice site $\mathbf{R}$ is then

$$H_{\mathbf{R}} = \omega_c^{\mathbf{R}} a_{\mathbf{R}}^\dagger a_{\mathbf{R}} + \omega_0^{\mathbf{R}} \sigma_+^{\mathbf{R}} \sigma_-^{\mathbf{R}} + g_{\mathbf{R}}(a_{\mathbf{R}}^\dagger + a_{\mathbf{R}})\sigma_x^{\mathbf{R}}, \tag{4.1}$$

where the Hamiltonian has been expressed in angular frequency units by dividing with $\hbar$, and $\omega_c^{\mathbf{R}}$ and $\omega_0^{\mathbf{R}}$ are the cavity frequency and qubit frequency splitting, respectively, at site $\mathbf{R}$. We will denote this with

$$H_{\mathbf{R}} = H_{\mathbf{R}}\Big[a_{\mathbf{R}}, a_{\mathbf{R}}^\dagger, \sigma_\pm^{\mathbf{R}}\Big]. \tag{4.2}$$

Let us first consider the symmetry properties of this single-site Hamiltonian. The Z_2 symmetry is associated with the parity operator

$$\Pi = e^{i\pi\mathcal{N}}, \tag{4.3}$$

where $\mathcal{N} = a^\dagger a + \sigma_+\sigma_-$. It can be shown that

$$\Pi^\dagger a \Pi = -a, \quad \Pi^\dagger a^\dagger \Pi = -a^\dagger \quad \text{and} \quad \Pi^\dagger \sigma_\pm \Pi = -\sigma_\pm. \tag{4.4}$$

Therefore, we can easily obtain

$$\Pi^\dagger x \Pi = -x \quad \text{and} \quad \Pi^\dagger H_{\mathbf{R}} \Pi = H_{\mathbf{R}} \tag{4.5}$$

because Π is unitary, $\Pi\Pi^\dagger = \Pi^\dagger\Pi = 1$. The action of the parity operator leaves the Hamiltonian invariant, from which it follows that Π and $H_{\mathbf{R}}$ commute,

$$[\Pi, H_{\mathbf{R}}] = 0. \tag{4.6}$$

The non-degenerate eigenstates $|n_{\mathbf{R}}\rangle$ of $H_{\mathbf{R}}$ are also the eigenstates of Π,

$$\Pi\,|n_{\mathbf{R}}\rangle = \pi_{n_{\mathbf{R}}}\,|n_{\mathbf{R}}\rangle\,, \tag{4.7}$$

where $\pi_{n_{\mathbf{R}}} = 1$ or $\pi_{n_{\mathbf{R}}} = -1$. In other words, the eigenstates $|n_{\mathbf{R}}\rangle$ have definite parity. It is now easy to show that this implies $\langle x\rangle = 0$. We obtain

$$\langle n_{\mathbf{R}}|x|n_{\mathbf{R}}\rangle = \langle n_{\mathbf{R}}|\Pi^\dagger\Pi x \Pi^\dagger\Pi|n_{\mathbf{R}}\rangle = -\pi_{n_{\mathbf{R}}}^2\,\langle n_{\mathbf{R}}|x|n_{\mathbf{R}}\rangle\,. \tag{4.8}$$

Thus it must be true that $\langle n_{\mathbf{R}}|x|n_{\mathbf{R}}\rangle = 0$.

Now consider the nonlinear coupling of the trapped ion Hamiltonian (3.72),

$$H_{\text{int}} = -g\cos\Big(\eta(a^\dagger + a) + \phi_{\text{ext}}\Big)\sigma_x. \tag{4.9}$$

Because odd powers of x have odd parity and its even powers even parity, the coupling has odd parity if $\phi_{\text{ext}} = l\pi$, where l is an integer. On the other hand, it has even parity if $\phi_{\text{ext}} = \pi/2 + l\pi$. If we choose the latter values of ϕ_{ext}, the trapped ion Hamiltonian will have the same Z_2 symmetry as the above linear Rabi Hamiltonian.

In the Rabi-Hubbard model, in which photons hop between neighboring lattice sites and interact locally with qubits, the interaction Hamiltonian between lattice sites $\mathbf{R}$ and $\mathbf{R}'$, called the hopping term, is of the form

$$H_{\text{hop}} = -J_{\mathbf{R}\mathbf{R}'}x_{\mathbf{R}}x_{\mathbf{R}'}, \tag{4.10}$$

where we have denoted $x_{\mathbf{R}} = a^\dagger_{\mathbf{R}} + a_{\mathbf{R}}$. The factor $J_{\mathbf{R}\mathbf{R}'}$ is the coupling constant between the lattice sites. We now get the full many-body Hamiltonian into the form

$$H = -\sum_{\langle \mathbf{R}\mathbf{R}'\rangle} J_{\mathbf{R}\mathbf{R}'}x_{\mathbf{R}}x_{\mathbf{R}'} + \sum_{\mathbf{R}} H_{\mathbf{R}}\Big[a_{\mathbf{R}}, a^\dagger_{\mathbf{R}}, \sigma^{\mathbf{R}}_{\pm}\Big]. \tag{4.11}$$

The sum $\langle \mathbf{R}\mathbf{R}'\rangle$ is taken over nearest neighbor pairs. This is what we will call the linear Rabi-Hubbard model.

If in equation (4.11) we set $J_{\mathbf{R}\mathbf{R}'} = 0$ for all pairs of $\mathbf{R}$ and $\mathbf{R}'$, all the lattice sites decouple and the problem is reduced to a collection of independent Rabi systems. If, on the other hand, all $g_{\mathbf{R}} = 0$, the photons are delocalized throughout the lattice and form a band. In the general case $J_{\mathbf{R}\mathbf{R}'} \neq 0$, $g_{\mathbf{R}} \neq 0$, the Rabi-Hubbard model cannot be solved exactly. We will proceed to analyze the situation by using mean field theory. [4]

4.2 Mean Field Theory

Following [4] and [34], let us write the mean field approximation for the hopping term. In this approach, we write $x_{\mathbf{R}}$ using its mean value $\langle x_{\mathbf{R}}\rangle$ and fluctuations $\delta x_{\mathbf{R}}$ about it,

$$x_{\mathbf{R}} = \langle x_{\mathbf{R}}\rangle + \delta x_{\mathbf{R}}. \tag{4.12}$$

We multiply the fluctuations with each other,

$$\delta x_{\mathbf{R}}\delta x_{\mathbf{R}'} = x_{\mathbf{R}}x_{\mathbf{R}'} - x_{\mathbf{R}}\langle x_{\mathbf{R}'}\rangle - \langle x_{\mathbf{R}}\rangle x_{\mathbf{R}'} + \langle x_{\mathbf{R}}\rangle\langle x_{\mathbf{R}'}\rangle. \tag{4.13}$$

This becomes

$$x_{\mathbf{R}}x_{\mathbf{R}'} - \delta x_{\mathbf{R}}\delta x_{\mathbf{R}'} = x_{\mathbf{R}}\langle x_{\mathbf{R}'}\rangle + \langle x_{\mathbf{R}}\rangle x_{\mathbf{R}'} - \langle x_{\mathbf{R}}\rangle\langle x_{\mathbf{R}'}\rangle . \tag{4.14}$$

Assuming the fluctuations are small, the hopping term can then be decoupled as

$$x_{\mathbf{R}}x_{\mathbf{R}'} \simeq x_{\mathbf{R}}\langle x_{\mathbf{R}'}\rangle + \langle x_{\mathbf{R}}\rangle x_{\mathbf{R}'} - \langle x_{\mathbf{R}}\rangle\langle x_{\mathbf{R}'}\rangle . \tag{4.15}$$

If we make the mean field approximation $\langle x_{\mathbf{R}}\rangle = \langle x\rangle$ and assume $J_{\mathbf{R}\mathbf{R}'} = J$ throughout the lattice, the hopping term takes the form

$$H_{\text{hop}} = -J\Big[x_{\mathbf{R}}\langle x\rangle + \langle x\rangle x_{\mathbf{R}'} - \langle x\rangle^2\Big]. \tag{4.16}$$

When this is summed over all the bonds $\langle \mathbf{R}\mathbf{R}'\rangle$, each term $\langle x\rangle x_{\mathbf{R}}$ is counted as many times as the number of its nearest neighbors and there are as many of the terms $-\langle x\rangle^2$ as there are bonds. The final Hamiltonian is

$$H = \sum_{\mathbf{R}}\left[H_{\mathbf{R}}\Big[a_{\mathbf{R}}, a^{\dagger}_{\mathbf{R}}, \sigma^{\mathbf{R}}_{\pm}\Big] - J\varphi(zx_{\mathbf{R}} - b\varphi)\right], \tag{4.17}$$

where $\varphi = \langle x\rangle$, z is the coordination number of the lattice, which gives the number of nearest neighbors of each lattice site, and b is the number of bonds per lattice site.

In general, consider a Hamiltonian of the form $H = \sum_i H_i$, where each H_i has an eigenstate ψ_i on which it exclusively operates, with eigenvalue ε_i. If we denote $\Psi = \prod_i \psi_i$,

$$H\Psi = \sum_i H_i \prod_i \psi_i = \sum_i \varepsilon_i \prod_i \psi_i = \sum_i \varepsilon_i \Psi. \tag{4.18}$$

As we can see, the full solution of a many-body problem described by such a Hamiltonian is simply constructed from the solutions of the one-body problems i.

In the mean field approximation (4.17), the lattice sites become independent, and the complicated many-body problem is therefore reduced to a simpler one-body problem. Assuming all sites are identical, it is sufficient to consider only a single site, omitting the site index $\mathbf{R}$.

4.3 Perturbative Method for the Phase Boundary

The critical value of the hopping J_c at which the lattice changes phase can be found by considering the mean-field hopping

$$H_1 = -J\varphi(zx - b\varphi) \tag{4.19}$$

to be a small perturbation to the single-site Hamiltonian

$$H_0 = \omega_c a^\dagger a + \omega_q \sigma_+ \sigma_- + gx\sigma_x \tag{4.20}$$

and writing the single-site energy using second-order non-degenerate perturbation theory [34]. We will denote the eigenvalues and eigenstates of the unperturbed Hamiltonian with $\varepsilon_0(n)$ and $|n\rangle$:

$$H_0 |n\rangle = \varepsilon_0(n) |n\rangle , \tag{4.21}$$

where $n = 1, 2, \ldots$. Assuming the states $|n\rangle$ are normalized, they form an orthonormal set and

$$\langle m|n\rangle = \delta_{mn}. \tag{4.22}$$

We will follow the standard approach (e.g. Cohen-Tannoudji et al. [35]) and write the Hamiltonian in the form

$$H = H_0 + \lambda H_1, \tag{4.23}$$

where λ is an arbitrary dimensionless parameter that will be set to 1 in the end. The eigenstates $|\psi_n\rangle$ and eigenvalues ε_n of H are expanded as

$$|\psi_n\rangle = \left|\psi_n^{(0)}\right\rangle + \lambda \left|\psi_n^{(1)}\right\rangle + \lambda^2 \left|\psi_n^{(2)}\right\rangle + \mathcal{O}(\lambda^3) \tag{4.24a}$$

$$\varepsilon_n = \varepsilon_n^{(0)} + \lambda\varepsilon_n^{(1)} + \lambda^2\varepsilon_n^{(2)} + \mathcal{O}(\lambda^3), \tag{4.24b}$$

where $\left|\psi_n^{(0)}\right\rangle = |n\rangle$ and $\varepsilon_n^{(0)} = \varepsilon_0(n)$. In addition, the vectors $\left|\psi_n^{(i)}\right\rangle$ must be orthogonal to $\left|\psi_n^{(0)}\right\rangle$. The expansions (4.24) must satisfy the equation

$$H |\psi_n\rangle = \varepsilon_n |\psi_n\rangle . \tag{4.25}$$

When the expansions (4.24) up to second order are substituted into equation (4.25) and higher than second-order terms discarded, we get

$$\begin{aligned}
&\lambda^0 \Big[H_0 \left|\psi_n^{(0)}\right\rangle - \varepsilon_n^{(0)} \left|\psi_n^{(0)}\right\rangle \Big] \\
&+ \lambda^1 \Big[H_0 \left|\psi_n^{(1)}\right\rangle + H_1 \left|\psi_n^{(0)}\right\rangle - \varepsilon_n^{(0)} \left|\psi_n^{(1)}\right\rangle - \varepsilon_n^{(1)} \left|\psi_n^{(0)}\right\rangle \Big] \\
&+ \lambda^2 \Big[H_0 \left|\psi_n^{(2)}\right\rangle + H_1 \left|\psi_n^{(1)}\right\rangle - \varepsilon_n^{(0)} \left|\psi_n^{(2)}\right\rangle - \varepsilon_n^{(1)} \left|\psi_n^{(1)}\right\rangle - \varepsilon_n^{(2)} \left|\psi_n^{(0)}\right\rangle \Big] \\
&= 0.
\end{aligned} \tag{4.26}$$

Because the parameter λ is arbitrary, the coefficient of each power of λ must be separately equal to zero. We therefore get the following conditions:

$$H_0 \left|\psi_n^{(0)}\right\rangle = \varepsilon_n^{(0)} \left|\psi_n^{(0)}\right\rangle \tag{4.27}$$

$$H_0\left|\psi_n^{(1)}\right\rangle + H_1\left|\psi_n^{(0)}\right\rangle = \varepsilon_n^{(0)}\left|\psi_n^{(1)}\right\rangle + \varepsilon_n^{(1)}\left|\psi_n^{(0)}\right\rangle \tag{4.28}$$

$$H_0\left|\psi_n^{(2)}\right\rangle + H_1\left|\psi_n^{(1)}\right\rangle = \varepsilon_n^{(0)}\left|\psi_n^{(2)}\right\rangle + \varepsilon_n^{(1)}\left|\psi_n^{(1)}\right\rangle + \varepsilon_n^{(2)}\left|\psi_n^{(0)}\right\rangle. \tag{4.29}$$

The first of these is simply a restatement of equation (4.21). The other two equations result in first- and second-order corrections to the unperturbed $\left|\psi_n^{(0)}\right\rangle$ and $\varepsilon_n^{(0)}$.

The first-order correction to the energy is found by multiplying equation (4.28) from the left with $\left\langle\psi_n^{(0)}\right|$, which results in

$$\left\langle\psi_n^{(0)}\middle|H_0\middle|\psi_n^{(1)}\right\rangle + \left\langle\psi_n^{(0)}\middle|H_1\middle|\psi_n^{(0)}\right\rangle = \varepsilon_n^{(1)}, \tag{4.30}$$

because $\left\langle\psi_n^{(0)}\middle|\psi_n^{(1)}\right\rangle = 0$. Also, because H_0 is Hermitian,

$$\left\langle\psi_n^{(0)}\middle|H_0\middle|\psi_n^{(1)}\right\rangle = \left\langle\psi_n^{(0)}\middle|H_0^\dagger\middle|\psi_n^{(1)}\right\rangle = \varepsilon_n^{(0)}\left\langle\psi_n^{(0)}\middle|\psi_n^{(1)}\right\rangle = 0. \tag{4.31}$$

The first-order correction to the energy is then

$$\varepsilon_n^{(1)} = \left\langle\psi_n^{(0)}\middle|H_1\middle|\psi_n^{(0)}\right\rangle. \tag{4.32}$$

To calculate the second-order energy correction, we need the first-order correction to the state $|\psi_n\rangle$. We begin by expanding $\left|\psi_n^{(1)}\right\rangle$ into the series

$$\left|\psi_n^{(1)}\right\rangle = \sum_{k\neq n} C_k\left|\psi_k^{(0)}\right\rangle \tag{4.33}$$

and substituting it into equation (4.28), which results in

$$\sum_{k\neq n} C_k\varepsilon_k^{(0)}\left|\psi_k^{(0)}\right\rangle + H_1\left|\psi_n^{(0)}\right\rangle = \varepsilon_n^{(0)}\sum_{k\neq n} C_k\left|\psi_k^{(0)}\right\rangle + \varepsilon_n^{(1)}\left|\psi_n^{(0)}\right\rangle. \tag{4.34}$$

Multiplying from the left with $\left\langle\psi_m^{(0)}\right|$, where $m \neq n$, gives

$$C_m\varepsilon_m^{(0)} + \left\langle\psi_m^{(0)}\middle|H_1\middle|\psi_n^{(0)}\right\rangle = \varepsilon_n^{(0)}C_m. \tag{4.35}$$

Rearranging this yields the expression for C_m:

$$C_m = \frac{\left\langle\psi_m^{(0)}\middle|H_1\middle|\psi_n^{(0)}\right\rangle}{\varepsilon_n^{(0)} - \varepsilon_m^{(0)}}. \tag{4.36}$$

Now the second-order energy correction can be found by multiplying equation (4.29) from the left with $\left\langle\psi_n^{(0)}\right|$, giving

$$\left\langle\psi_n^{(0)}\middle|H_0\middle|\psi_n^{(2)}\right\rangle + \left\langle\psi_n^{(0)}\middle|H_1\middle|\psi_n^{(1)}\right\rangle = \varepsilon_n^{(2)}. \tag{4.37}$$

The first term on the left is zero by the same argument as before, so

$$\varepsilon_n^{(2)} = \left\langle \psi_n^{(0)} \middle| H_1 \middle| \psi_n^{(1)} \right\rangle . \tag{4.38}$$

We can now substitute the expansion for $\left|\psi_n^{(1)}\right\rangle$ calculated before,

$$\begin{aligned}
\varepsilon_n^{(2)} &= \left\langle \psi_n^{(0)} \middle| H_1 \middle| \sum_{k\neq n} C_k \psi_k^{(0)} \right\rangle \\
&= \sum_{k\neq n} C_k \left\langle \psi_n^{(0)} \middle| H_1 \middle| \psi_k^{(0)} \right\rangle \\
&= \sum_{k\neq n} \frac{\left\langle \psi_k^{(0)} \middle| H_1 \middle| \psi_n^{(0)} \right\rangle}{\varepsilon_n^{(0)} - \varepsilon_k^{(0)}} \left\langle \psi_n^{(0)} \middle| H_1 \middle| \psi_k^{(0)} \right\rangle \\
&= \sum_{k\neq n} \frac{\left\langle \psi_k^{(0)} \middle| H_1 \middle| \psi_n^{(0)} \right\rangle}{\varepsilon_n^{(0)} - \varepsilon_k^{(0)}} \left\langle \psi_k^{(0)} \middle| H_1^\dagger \middle| \psi_n^{(0)} \right\rangle^* \\
&= \sum_{k\neq n} \frac{\left| \left\langle \psi_k^{(0)} \middle| H_1 \middle| \psi_n^{(0)} \right\rangle \right|^2}{\varepsilon_n^{(0)} - \varepsilon_k^{(0)}},
\end{aligned} \tag{4.39}$$

because H_1 is Hermitian. The expression for the energy in second-order perturbation theory is therefore

$$\varepsilon_n = \varepsilon_n^{(0)} + \left\langle \psi_n^{(0)} \middle| H_1 \middle| \psi_n^{(0)} \right\rangle + \sum_{k\neq n} \frac{\left| \left\langle \psi_k^{(0)} \middle| H_1 \middle| \psi_n^{(0)} \right\rangle \right|^2}{\varepsilon_n^{(0)} - \varepsilon_k^{(0)}}, \tag{4.40}$$

or, returning to our notation of the Rabi-Hubbard model,

$$\varepsilon(n) = \varepsilon_0(n) + \langle n|H_1|n\rangle + \sum_{k\neq n} \frac{|\langle k|H_1|n\rangle|^2}{\varepsilon_0(n) - \varepsilon_0(k)}. \tag{4.41}$$

The mean field energy of the whole lattice is simply $N\varepsilon(n)$, where N is the number of lattice sites, assuming all the sites are identical.

The first-order correction to the single-site energy is

$$\langle n|H_1|n\rangle = -J\varphi \langle n|(zx - b\varphi)|n\rangle = Jb\varphi^2, \tag{4.42}$$

because $\langle n|x|n\rangle = 0$ in the linear Rabi model [4]. The second-order correc-

tion is

$$\begin{aligned}\sum_{k\neq n}\frac{|\langle k|H_1|n\rangle|^2}{\varepsilon_0(n)-\varepsilon_0(k)} &= (J\varphi)^2\sum_{k\neq n}\frac{|\langle k|(zx-b\varphi)|n\rangle|^2}{\varepsilon_0(n)-\varepsilon_0(k)}\\ &= -(J\varphi)^2 z\sum_{k\neq n}\frac{|\langle k|x|n\rangle|^2}{\varepsilon_0(k)-\varepsilon_0(n)}\\ &= -(J\varphi)^2 z\mathcal{F}(n),\end{aligned} \tag{4.43}$$

where we have used the definition

$$\mathcal{F}(n)=\sum_{k\neq n}\frac{|\langle k|x|n\rangle|^2}{\varepsilon_0(k)-\varepsilon_0(n)}. \tag{4.44}$$

We can now write the perturbed single-site energy up to second order as

$$\varepsilon(n)=\varepsilon_0(n)+Jb\varphi^2-(J\varphi)^2 z\mathcal{F}(n)=\varepsilon_0(n)+J\varphi^2\Big[b-Jz\mathcal{F}(n)\Big]. \tag{4.45}$$

If $Jz\mathcal{F}(n)<b$, the energy (4.45) is minimized when $\varphi=0$ (disordered phase). If, on the other hand, $Jz\mathcal{F}(n)>b$, the energy is minimized when φ is nonzero (ordered phase). We therefore expect that at zero temperature, a phase transition occurs at the critical hopping

$$J_c=\frac{b}{z\mathcal{F}(n)} \tag{4.46}$$

and φ is the order parameter of this transition. It should in principle be determined self-consistently in the ground state of the single-site mean field Hamiltonian [34]. The phase boundary of a linear, one-dimensional ($z=2$, $b=1$) Rabi-Hubbard lattice is shown in figure 4.1, calculated with different values of the detuning $\delta=\omega_0-\omega_c$. We see that a disordered phase with Z_2 symmetry is stable until the critical hopping strength is reached. At this point, a transition toward an ordered phase occurs and the symmetry is spontaneously broken. As ω_0 grows, it tends to cause stronger quantum fluctuations in the qubit, which favors local disordering [4]. This is why the region of the ordered broken symmetry phase shrinks with growing detuning as seen in figure 4.1.

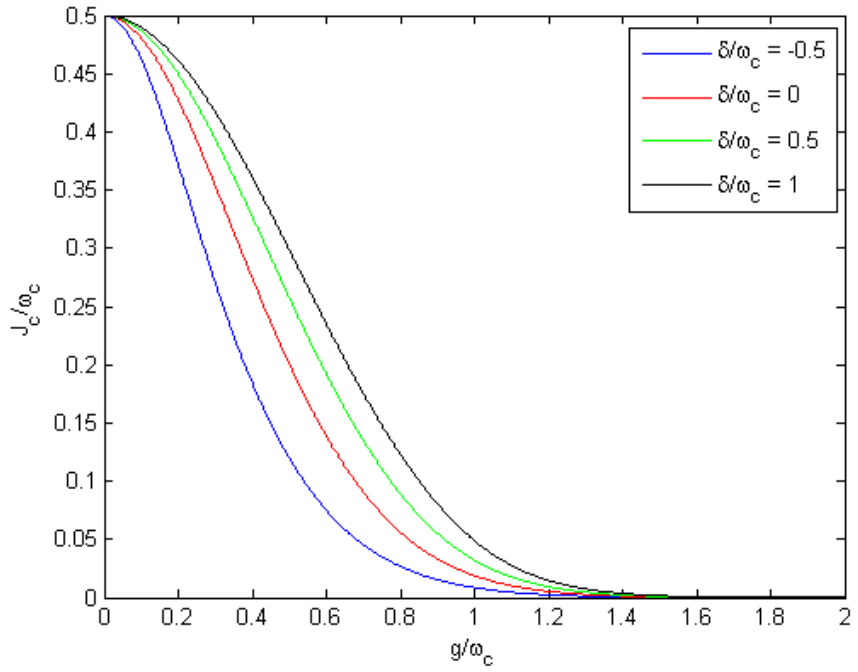

Figure 4.1: Phase boundary of the linear Rabi-Hubbard lattice in the mean field approximation with $\omega_c/2\pi = 3.5$ GHz, showing the critical value of the hopping J_c as a function of the coupling g. The phase boundary has been calculated for different values of the scaled detuning $\delta/\omega_c = (\omega_0 - \omega_c)/\omega_c$. The linear Rabi Hamiltonian (4.1) was approximated as a 20×20 matrix to calculate this figure numerically.

Chapter 5

Nonlinear Rabi-Hubbard Model

In the previous chapter, we discussed the Rabi-Hubbard model in the context of a lattice formed by linear CQED elements, and presented the phase diagram of such a system. Now we will proceed to study how the situation changes if the linear elements are replaced with nonlinear artificial trapped ions introduced in section 3.3. The formulas derived for the linear Rabi-Hubbard model can be straightforwardly applied to this case. We will consider a one-dimensional lattice for which $z = 2$, $b = 1$. In order to calculate results, we must first solve the single-site eigenvalue problem defined by the ion trap Hamiltonian (3.72). This can be done numerically. Some single-site properties will also be calculated. Of particular interest is the value of $\langle x \rangle$, which vanishes due to symmetry in the linear model. It should also vanish with the trapped ion Hamiltonian with the right values of ϕ_{ext}. Finally, we will solve the phase boundary, also numerically, using equation (4.46).

In the following calculations, we will use the same experimentally achievable parameters as before in section 3.3.4: $\omega_c/2\pi = 3.5$ GHz and $L = 410$ pH, from which η is calculated to be $\eta \approx 0.03$. However, it was shown in Ref. [28] that the nonlinearity of the interaction becomes significant at around $\eta \approx 0.2$. We will therefore use this in our calculations unless otherwise stated, expecting such values are possible to reach with optimization in the fabrication process. From Ref. [31], we also use the value $E_{J0}/h = 27$ GHz, which gives $g/2\pi \approx 14$ GHz. For ϕ_{ext}, we choose the value $\phi_{\text{ext}} = \pi/2$, since this choice results in the same Z_2 symmetry as in

the linear model and transforms the coupling Hamiltonian into

$$H_{0,\mathrm{int}} = g \sin\Big(\eta(a^\dagger + a)\Big)\sigma_x. \tag{5.1}$$

Its series expansion is

$$H_{0,\mathrm{int}} = g\Big(\eta(a^\dagger + a) - \eta^3(a^\dagger + a)^3/3! + \dots\Big)\sigma_x. \tag{5.2}$$

If η is small, all the nonlinear terms can be discarded. The interaction is then reduced into the Rabi model,

$$H_{0,\mathrm{int}} \approx g\eta(a^\dagger + a)\sigma_x, \tag{5.3}$$

which was used by Schiró et al. [4] in calculating the linear Rabi-Hubbard phase boundary. The only difference is that the interaction is weakened by factor η.

5.1 Single-Site Properties

Let us explicitly state the problem to be solved: the eigenequation is

$$H_0 \left|m\right\rangle = \varepsilon_0(m) \left|m\right\rangle, \tag{5.4}$$

where we have used the index m to label the single-site eigenstates to avoid confusion with the oscillator states and

$$H_0 = \omega_c a^\dagger a + \frac{\omega_0}{2}\sigma_z - g\cos\Big(\eta(a^\dagger + a) + \phi_{\mathrm{ext}}\Big)\sigma_x \tag{5.5}$$

is the single-site Hamiltonian and $\varepsilon_0(n)$ are the eigenvalues and $|n\rangle$ the corresponding eigenvectors to be determined.

In order to solve the problem numerically, the Hamiltonian (5.5) is represented in matrix form in the basis $\{|\alpha, n\rangle = |\alpha\rangle \otimes |n\rangle, \alpha = g, e \text{ and } n = 0, 1, 2, \dots\}$, where $|\alpha\rangle$ are the eigenstates of the ground (g) and excited (e) states of the qubit, and $|n\rangle$ are the eigenstates of the oscillator. The resulting infinite matrix is truncated to include only the lowest twenty oscillator states, leaving a 40×40 matrix, from which the single-site eigenstates and eigenenergies are calculated.

In the matrix elements of the Hamiltonian, the first two terms of (5.5) contribute the eigenenergies of the qubit and the oscillator on the diagonal,

and nothing elsewhere, giving the simple diagonal matrix

$$H_{0,\text{diag}} = \begin{pmatrix} -\frac{\omega_0}{2} & 0 & 0 & 0 & 0 & 0 & \dots \\ 0 & \frac{\omega_0}{2} & 0 & 0 & 0 & 0 & \dots \\ 0 & 0 & -\frac{\omega_0}{2}+\omega_c & 0 & 0 & 0 & \dots \\ 0 & 0 & 0 & \frac{\omega_0}{2}+\omega_c & 0 & 0 & \dots \\ 0 & 0 & 0 & 0 & -\frac{\omega_0}{2}+2\omega_c & 0 & \dots \\ 0 & 0 & 0 & 0 & 0 & \frac{\omega_0}{2}+2\omega_c & \dots \\ \vdots & \vdots & \vdots & \vdots & \vdots & \vdots & \ddots \end{pmatrix}. \tag{5.6}$$

This leaves calculating the matrix elements of the interaction term. The effect of the operator $\sigma_x = \sigma_+ + \sigma_-$ is to raise a qubit in the ground state to the excited state and vice versa. The matrix elements of the remaining cosine operator, which we will denote

$$g(x) = \cos\Big(\eta(a^\dagger + a) + \phi_{\text{ext}}\Big), \tag{5.7}$$

are stated in Ref. [24, 36] to be, for elements of the form $\langle n|g(x)|n+k\rangle$,

$$\langle n|g(x)|n+k\rangle = (e^{i\phi_{\text{ext}}} + (-1)^k e^{-i\phi_{\text{ext}}})(i\eta)^k \sqrt{\frac{n!}{(n+k)!}} L_n^k(\eta^2) e^{-\eta^2/2}, \tag{5.8}$$

where $L_n^k(\eta^2)$ is an associated Laguerre polynomial. The remaining matrix elements can easily be obtained by using the Hermiticity of $g(x)$:

$$\begin{aligned} \langle n+k|g(x)|n\rangle &= \langle n|g(x)|n+k\rangle^* \\ &= ((-1)^k e^{-i\phi_{\text{ext}}} + e^{i\phi_{\text{ext}}})(i\eta)^k \sqrt{\frac{n!}{(n+k)!}} L_n^k(\eta^2) e^{-\eta^2/2} \\ &= \langle n|g(x)|n+k\rangle\,. \end{aligned} \tag{5.9}$$

The interaction matrix is then of the form

$$H_{0,\text{int}} = -g \begin{pmatrix} 0 & \langle 1|g(x)|1\rangle & 0 & \langle 1|g(x)|2\rangle & 0 & \langle 1|g(x)|3\rangle & \dots \\ \langle 1|g(x)|1\rangle & 0 & \langle 1|g(x)|2\rangle & 0 & \langle 1|g(x)|3\rangle & 0 & \dots \\ 0 & \langle 2|g(x)|1\rangle & 0 & \langle 2|g(x)|2\rangle & 0 & \langle 2|g(x)|3\rangle & \dots \\ \langle 2|g(x)|1\rangle & 0 & \langle 2|g(x)|2\rangle & 0 & \langle 2|g(x)|3\rangle & 0 & \dots \\ 0 & \langle 3|g(x)|1\rangle & 0 & \langle 3|g(x)|2\rangle & 0 & \langle 3|g(x)|3\rangle & \dots \\ \langle 3|g(x)|1\rangle & 0 & \langle 3|g(x)|2\rangle & 0 & \langle 3|g(x)|3\rangle & 0 & \dots \\ \vdots & \vdots & \vdots & \vdots & \vdots & \vdots & \ddots \end{pmatrix}. \tag{5.10}$$

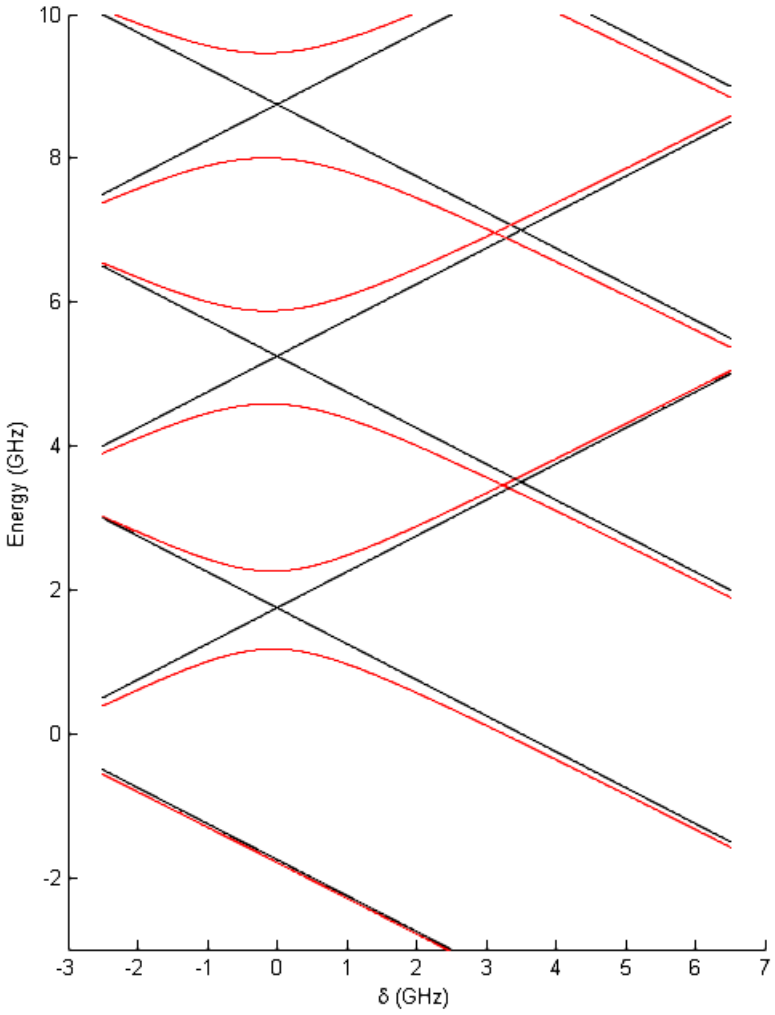

Figure 5.1: Plot of the eigenenergies of the Hamiltonian (5.5) in red as a function of the detuning $\delta = \omega_0 - \omega_c$. A weaker coupling of $g/2\pi = 1$ GHz was used in this figure to make the effect of the interaction clearer. The eigenenergies of the uncoupled system ($g = 0$) are plotted in black.

Some of the lowest eigenenergies obtained this way are shown in figure 5.1.

At $\delta = 0$, the eigenenergies of the states $|e, n\rangle$ and $|g, n+1\rangle$ become degenerate in the uncoupled system. The degeneracy vanishes with the introduction of coupling, a phenomenon known as avoided crossings. However, we can see that the crossings of the states $|e, n\rangle$ and $|g, n+2\rangle$ at higher δ remain even in the presence of the coupling. This happens because the interaction Hamiltonian does not couple these states - they would be coupled by even-order terms of $a^\dagger + a$, which are not present with our choice of ϕ_{ext}. Avoided crossings do appear for the states $|e, n\rangle$ and $|g, n+3\rangle$, as they are coupled by terms of order three, five, and so on. The same pattern continues for yet higher avoided crossings, with the gaps becoming smaller and smaller as the minimum order of the terms coupling the states in question grows.

It is useful at this point to express the annihilation and creation operators a and $a^\dagger$ as matrices in the same basis as the Hamiltonian. The matrix elements of a are easily obtained from relation (2.13):

$$\langle \alpha, k|a|\beta, n\rangle = \sqrt{n}\,\langle \alpha, k|\beta, n-1\rangle = \sqrt{n}\delta_{\alpha,\beta}\delta_{k,n-1}. \tag{5.11}$$

This gives the matrix representation of the annihilation operator,

$$a = \begin{pmatrix} 0 & 0 & \sqrt{1} & 0 & 0 & 0 & \dots \\ 0 & 0 & 0 & \sqrt{1} & 0 & 0 & \dots \\ 0 & 0 & 0 & 0 & \sqrt{2} & 0 & \dots \\ 0 & 0 & 0 & 0 & 0 & \sqrt{2} & \dots \\ 0 & 0 & 0 & 0 & 0 & 0 & \dots \\ 0 & 0 & 0 & 0 & 0 & 0 & \dots \\ \vdots & \vdots & \vdots & \vdots & \vdots & \vdots & \ddots \end{pmatrix}. \tag{5.12}$$

The creation operator is the Hermitian conjugate of a,

$$a^\dagger = \begin{pmatrix} 0 & 0 & 0 & 0 & 0 & 0 & \dots \\ 0 & 0 & 0 & 0 & 0 & 0 & \dots \\ \sqrt{1} & 0 & 0 & 0 & 0 & 0 & \dots \\ 0 & \sqrt{1} & 0 & 0 & 0 & 0 & \dots \\ 0 & 0 & \sqrt{2} & 0 & 0 & 0 & \dots \\ 0 & 0 & 0 & \sqrt{2} & 0 & 0 & \dots \\ \vdots & \vdots & \vdots & \vdots & \vdots & \vdots & \ddots \end{pmatrix}. \tag{5.13}$$

With these, calculating matrix elements of operators constructed of a and $a^\dagger$ becomes the simple operation of matrix multiplication. For now, we solve

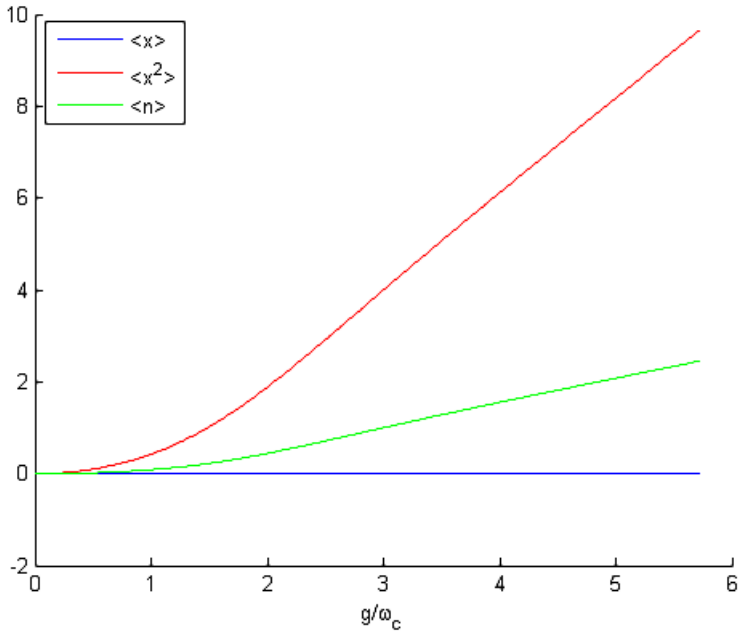

Figure 5.2: Comparison of $\langle x \rangle$, $\langle x^2 \rangle$ and $\langle \hat{n} \rangle = \langle a^\dagger a \rangle$ in the ground state with zero detuning $\delta = 0$.

the behavior of the expectation values $\langle x \rangle$, $\langle x^2 \rangle$ and $\langle a^\dagger a \rangle$ in the ground state $m = 1$, which means calculating the matrix elements $\langle 1|a + a^\dagger|1\rangle$, $\langle 1|(a + a^\dagger)^2|1\rangle$ and $\langle 1|a^\dagger a|1\rangle$. A comparison of these three is shown in figure 5.2. In figures 5.3 and 5.4, $\langle x^2 \rangle$ and $\langle a^\dagger a \rangle$ are plotted with different values of the detuning δ. The same expectation values are plotted with increasing values of η in figures 5.5 and 5.6, using zero detuning.

Right away we note that $\langle x \rangle$ vanishes in the nonlinear model, just as it does in the linear Rabi model. The result holds with any values of η and δ, not just the ones used here. We expected as much from symmetry arguments, and have now confirmed it numerically. This means that the perturbation method written for the linear Rabi-Hubbard phase boundary in section 4.3 is applicable to the nonlinear case without any need for modifications.

In the limit of small η, $\langle x^2 \rangle$ and $\langle a^\dagger a \rangle$ grow approximately quadratically, as a function of g. As η increases and the system becomes more nonlinear, asymptotic behavior begins to appear, the curve starting out as quadratic and apparently approaching a maximum value. Up to at least $\eta = 0.5$, $\langle x^2 \rangle$

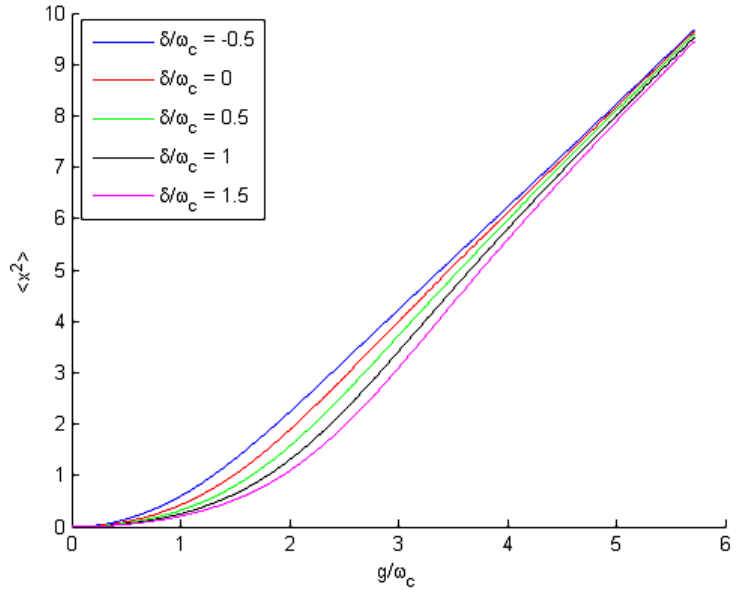

Figure 5.3: Plot of $\langle x^2 \rangle$ with different values of the scaled detuning δ/ω_c.

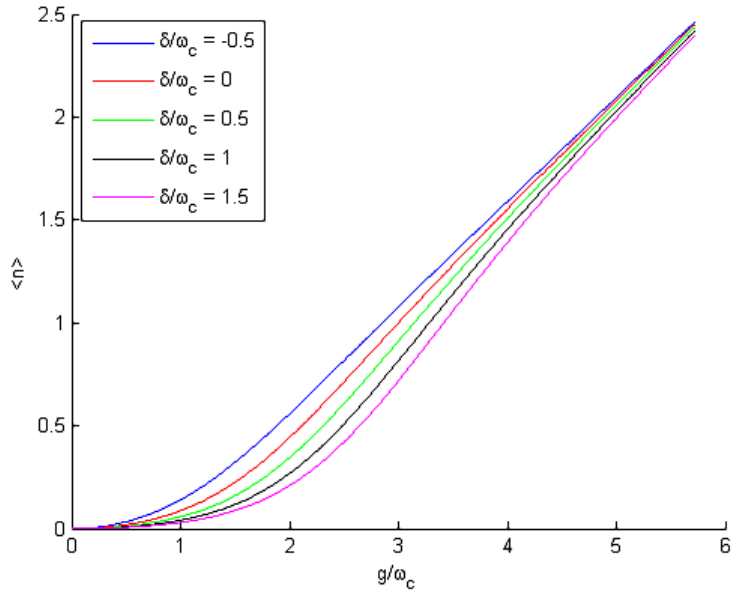

Figure 5.4: Plot of $\langle a^\dagger a \rangle$ with different values of the scaled detuning δ/ω_c.

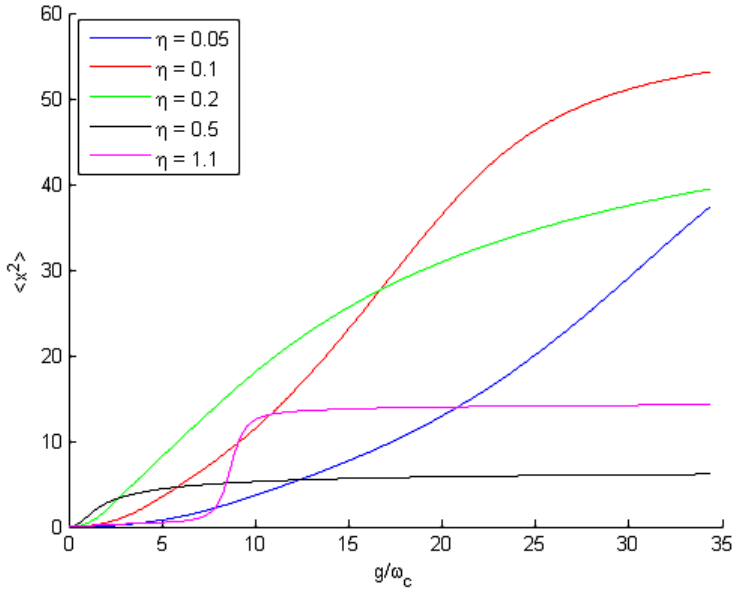

Figure 5.5: Plot of $\langle x^2 \rangle$ with different values of η and zero detuning $\delta = 0$.

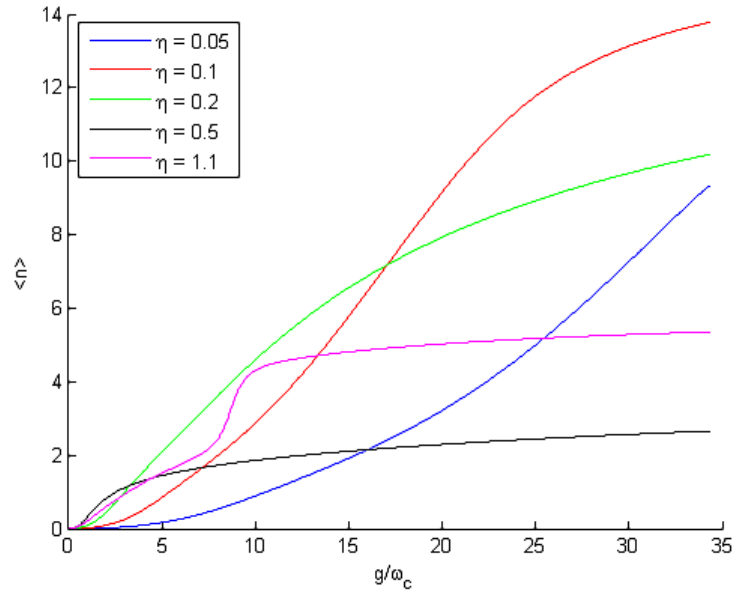

Figure 5.6: Plot of $\langle a^\dagger a \rangle$ with different values of η and zero detuning $\delta = 0$.

and $\langle a^\dagger a \rangle$ behave almost identically apart from a difference in scale. With values of η close to unity, the asymptotic behavior is more apparent and the curves of $\langle x^2 \rangle$ and $\langle a^\dagger a \rangle$ become more distinct compared to each other.

Nonlinear behavior with the parameters studied here only becomes clear with large values of the coupling constant g. With small values of g, the plots of $\langle x^2 \rangle$ and $\langle a^\dagger a \rangle$ tend to qualitatively resemble the linear curve.

5.2 Phase Boundary

In section 4.3, we derived the Rabi-Hubbard mean field phase boundary using perturbation theory and assuming $\langle x \rangle = 0$, which is true in the Rabi model. In the previous section, we found this assumption to hold in the nonlinear model of the artificial trapped ion as well. The analysis is therefore directly applicable here, as we made no other assumptions about the single-site properties. We are interested in the phase boundary of a one-dimensional lattice in the single-site ground state $m = 1$, for which the critical hopping is

$$J_c = \frac{1}{2\mathcal{F}(1)}, \tag{5.14}$$

where

$$\mathcal{F}(1) = \sum_{k \neq 1} \frac{|\langle k|x|1\rangle|^2}{\varepsilon_0(k) - \varepsilon_0(1)}. \tag{5.15}$$

Figure 5.7 shows the phase boundary calculated with a low value of η, for which the single-site coupling term is nearly linear. The result is consistent with the linear Rabi-Hubbard phase boundary in figure 4.1, which was to be expected. In figure 5.8, we have plotted the critical hopping as a function of η with three different values of g, first with 40 states as the basis set and again with an 80-state basis. We see that the two curves agree for all three values of the parameter g until $\eta \approx 2.5$, after which they become divergent. This indicates that approximating the Hamiltonian as a 40×40 matrix is a good approximation until then. Features seen before $\eta \approx 2.5$ can therefore comfortably be expected to be real effects, while any features seen at higher values of η may be numerical errors caused by the insufficiency of the basis set and cannot fully be trusted. However, the phase boundaries calculated with both basis sets reach a constant value of $J_c/\omega_c = 0.5$ at very high values of η, indicating this kind of saturation does in fact occur.

At first, increasing η causes the region of the broken symmetry phase to expand, until the progress is reversed at $\eta \approx 0.7$. At $\eta \approx 1.1$, a small peak

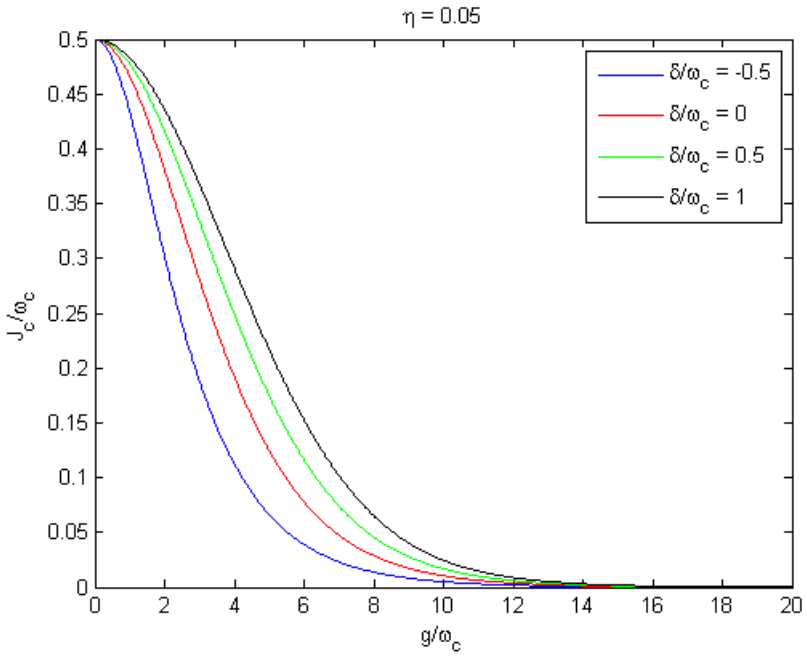

Figure 5.7: Critical hopping frequency J_c as a function of g with $\eta = 0.05$ with different values of the scaled detuning $\delta/\omega_c = (\omega_0 - \omega_c)/\omega_c$. We can see the same shape as the one calculated for the linear model in figure 4.1.

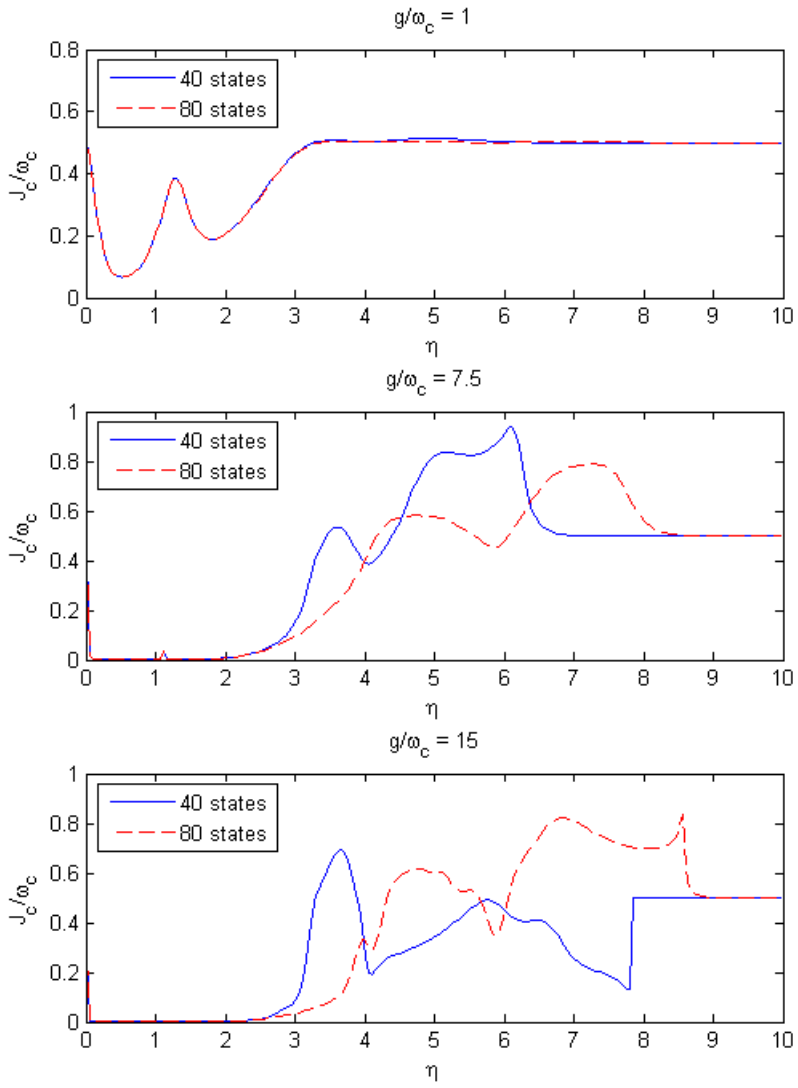

Figure 5.8: Critical hopping frequency J_c as a function of η with $\delta = 0$ for $g/\omega_c = 1$, $g/\omega_c = 7.5$ and $g/\omega_c = 15$, both with a 40-state basis set and an 80-state basis. The curves for all three values of the parameter g are identical until $\eta \approx 2.5$, after which the smaller approximation breaks down.

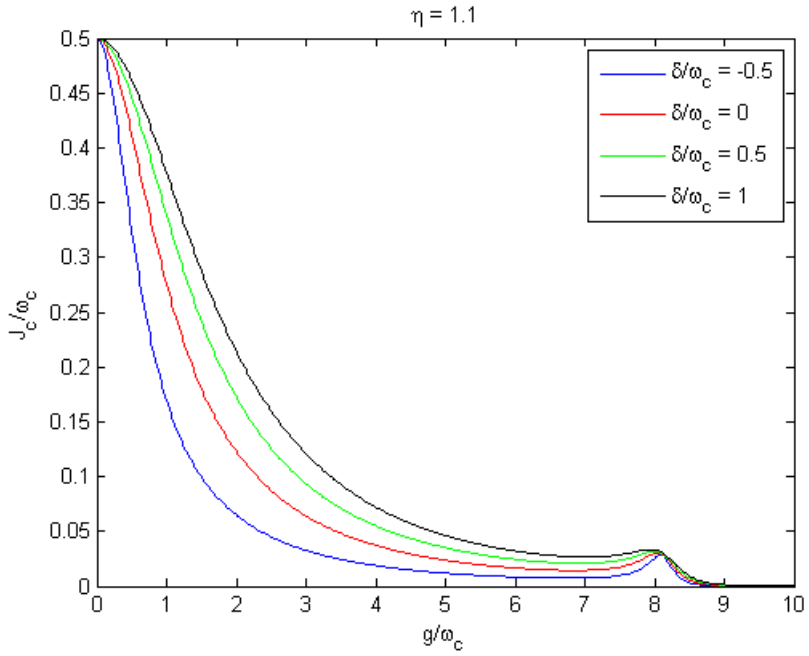

Figure 5.9: Critical hopping frequency J_c as a function of g with $\eta = 1.1$. Note the peak appearing at the end of the basic linear shape, corresponding to the maximum expansion of the broken symmetry phase as seen in figure 5.10.

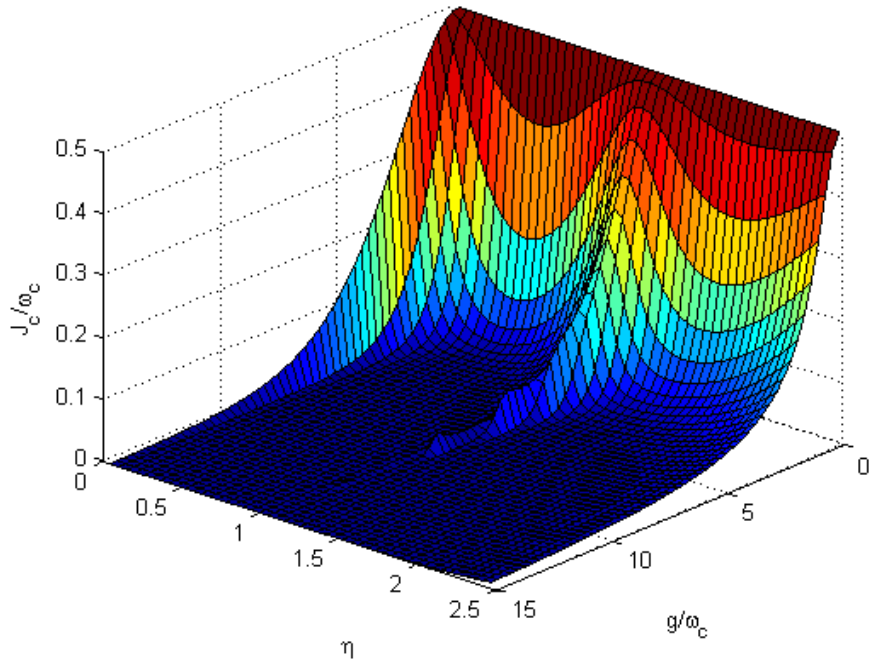

Figure 5.10: Critical hopping J_c as a function of g and η with zero detuning $\delta = 0$.

appears around a somewhat high value of $g/\omega_c \approx 8.1$, as seen in figure 5.9. This is a rather interesting phenomenon as elsewhere the system universally favors the broken symmetry phase more and more with growing coupling g. After the peak, the area of broken symmetry expands once more, before reversing again. This kind of oscillatory behavior must be a consequence of the sinusoidal coupling.

Comparing the plots in figure 5.8, J_c appears to oscillate before becoming saturated in all three cases, interestingly reaching a constant value equal to that of the uncoupled ($g = 0$) system. The process happens earlier for the lowest value of g. The reason for this can be seen from the analytical expression for the coupling matrix elements (5.8). The coupling strength is effectively $g/e^{\eta^2/2}$, which goes to zero with high η. As g increases, η must also increase to result in the same effective coupling. This explains why J_c is saturated earlier with lower values of g and why it reaches a constant value equivalent to the uncoupled case.

In figure 5.10, we have calculated the phase boundary as a function of g and η in the range $g/\omega_c \in [0, 15]$, $\eta \in [0.05, 2.5]$ to show its evolution with increasing η more clearly. This figure shows how the peak merges into the rest of the curve as η rises above $\eta = 1.1$.

The effect of adding π to the argument of

$$g(x) = \cos\Big(\eta(a^\dagger + a) + \phi_{\text{ext}}\Big), \tag{5.16}$$

in the coupling Hamiltonian is $g(x + \pi) = -g(x)$. It turns out that the sign of the coupling has no effect on $\mathcal{F}(1)$. Numerical calculations confirm $\mathcal{F}(1)$ is indeed periodic over the interval π. The phase boundaries we have calculated for $\phi_{\text{ext}} = \pi/2$ are therefore a general solution for all allowed ϕ_{ext} that preserve the Z_2 symmetry of the system.

Chapter 6

Conclusion

We studied the Hamiltonian of a single Cooper pair transistor coupled to an LC resonator and found it to be equivalent to the Hamiltonian of a real ion trap. Thus we confirmed that this kind of circuit can function as an artificial trapped ion.

The exact model of the Rabi-Hubbard lattice is a generally unsolvable many-body problem. Making the mean field approximation decouples the lattice sites and transforms the situation into a much simpler one-body problem, from which we derived the phase boundary using second-order perturbation theory.

In the course of calculating some single-site properties for the artificial trapped ion, we confirmed that $\langle a^\dagger + a \rangle = 0$ as suggested by symmetry, like it is in the linear Rabi model. This means that the perturbative method for deriving the phase boundary is the same in both cases. We also calculated $\langle (a^\dagger + a)^2 \rangle$ and $\langle a^\dagger a \rangle$ as a function of the coupling g, finding that nonlinearity alters their curves from quadratic to asymptotic, and that their behavior becomes qualitatively distinct only when the Lamb-Dicke parameter η rises close to unity.

In the nonlinear Rabi-Hubbard phase boundary, we discovered the presence of a single peak around $g/\omega_c \approx 8.1$ in addition to the linear curve shape when $\eta = 1.1$. There the broken symmetry phase emerges at a higher hopping strength, against the general trend of decreasing critical hopping with increasing g. We determined the 20-oscillator-state approximation used in most of our calculations to be good until $\eta \approx 2.5$. The phase boundary exhibits a kind of oscillatory behavior as a function of η before becoming saturated at high values of η.

For further study, one might investigate the effects nonhomogeneity in

the lattice by adding lattice sites with differing parameters. The possibility of other phase transitions when ϕ_{ext} is chosen so that the system lacks Z_2 symmetry may also warrant further research.

References

[1] R. O. Umucallar, I. Carusotto, Phys. Rev. A **84**, 043804 (2011).

[2] J. Cho, D. G. Angelakis, S. Bose, Phys. Rev. Lett. **101**, 246809 (2008).

[3] S. Schmidt, J. Koch, Ann. Phys. (Berlin) **525**, 395 (2013).

[4] M. Schiró, M. Bordyuh, B. Öztop, H. E. Türeci, J. Phys. B **46**, 224021 (2013).

[5] M. Schiró, M. Bordyuh, B. Öztop, H. E. Türeci, Phys. Rev. Lett. **109**, 053601 (2012).

[6] G. Zhu, S. Schmidt, J. Koch, New J. Phys. **15**, 115002 (2013).

[7] M. Schiró, C. Joshi, M. Bordyuh, R. Fazio, J. Keeling, H. E. Türeci, arXiv:1503.04456v1, (2015).

[8] M. A. Sillanpää, L. Roschier, P. J. Hakonen, Phys. Rev. Lett. **93**, 066805 (2004).

[9] B. M. Rodriguez-Lara, F. Soto-Eguibar, A. Zarate Cardenas, H. M. Moya-Cessa, Opt. Exp. **21**, 12888 (2013).

[10] E. Thuneberg, *Quantum Optics in Electric Circuits*, lecture notes, University of Oulu (2013).

[11] D. F. Walls, G. J. Milburn, *Quantum Optics*, 2nd edition. Brisbane: Springer-Verlag Berlin Heidelberg; 2008.

[12] A. Blais, R. Huang, A. Wallraff, S. M. Girvin, R. J. Schoelkopf, Phys. Rev. A **69**, 062320 (2004).

[13] H. Mabuchi, A. Doherty, Science **298**, 1372 (2002).

[14] A. Wallraff, D. I. Schuster, A. Blais, L. Frunzio, R. S. Huang, J. Majer, S. Kumar, S.M. Girvin, R. J. Schoelkopf, Nature **431**, 162 (2004).

[15] R. Blatt, D. Wineland, Nature **453**, 1008 (2008).

[16] J. Tuorila, M. Silveri, M. Sillanpää, E. Thuneberg, Y. Makhlin, P. Hakonen, Supercond. Sci. Technol. **26**, 124001 (2013).

[17] T. T. Heikkilä, F. Massel, J. Tuorila, R. Khan, M. A. Sillanpää, Phys. Rev. Lett. **112**, 203603 (2014).

[18] J. M. Pirkkalainen, S. U. Cho, F. Massel, J. Tuorila, T. T. Heikkilä, P. J. Hakonen, M. A. Sillanpää, Nature Communications **6**, 6981 (2015).

[19] T. E. Northup, K. M. Birnbaum, A. Boca, A. D. Boozer, J. McKeever, R. Miller, H. J. Kimble (2005) *Cavity QED with Single Atoms and Photons*. In: Atomic physics 19: XIX International Conference on Atomic Physics: ICAP 2004, Rio de Janeiro, Brazil, 25-30 July, 2004. American Institute of Physics Conference Proceedings. No.770. American Institute of Physics, Melville, NY, pp. 313-322.

[20] H. J. Kimble, Physica Scripta **T76**, 127 (1998).

[21] E. T. Jaynes, F. W. Cummings, Proc. IEEE **51**, 89 (1963).

[22] I. I. Rabi, Phys. Rev. **49**, 324 (1936).

[23] D. Leibfried, R. Blatt, C. Monroe, D. Wineland, Rev. Mod. Phys. **75** 281 (2003).

[24] W. Vogel, R. L. de Matos Filho, Phys. Rev. A **52**, 4214 (1995).

[25] J. Tuorila, *Spectroscopy of Artificial Atoms and Molecules*, Ph.D. Thesis, University of Oulu (2010).

[26] B. Yurke, J. S. Denker, Phys. Rev. A **29**, 1419 (1984).

[27] M. Devoret, *Quantum Fluctuations in Electrical Circuits*, Les Houches Session LXIII (1995).

[28] I. Pietikäinen, *Generalized Bloch-Siegert shift in an artificial trapped ion*, M.Sc. Thesis, University of Oulu (2014).

[29] H. D. Young, R. D. Freedman, *Sears and Zemansky's University Physics*, 12th edition. San Francisco: Pearson Addison-Wesley; 2008.

[30] A. G. Webster, *The Theory of Electricity and Magnetism; Being Lectures on Mathematical Physics*. London: Macmillan and co., Limited; 1897.

[31] J. Tuorila, M. Silveri, M. Sillanpää, E. Thuneberg, Yu. Makhlin, P. Hakonen, Phys. Rev. Lett. **105**, 257003 (2010).

[32] I. M. Georgescu, S. Ashhab, F. Nori, Rev. Mod. Phys. **86**, 153 (2014).

[33] A. Trabesinger, J. I. Cirac, P. Zoller, I. Bloch, J. Dalibard, S. Nascimbéne, R. Blatt, C. F. Roos, A. Aspuru-Guzik, P. Walther, A. A. Houck, H. E. Türeci, J. Koch, Nature Physics Insight **8**, 263-299 (2012).

[34] T. Sowinski, R. W. Chhajlany, arXiv:1404.0704v1 (2014).

[35] C. Cohen-Tannoudji, B. Diu, F. Laloë, *Quantum Mechanics*. Paris: Hermann; 1977.

[36] R. Onofrio, L. Viola, Phys. Rev. A **56**, 39 (1997).